ACS Catalysis

Research Article

pubs.acs.org/acscatalysis

Iron Complexes for the Electrocatalytic Oxidation of Hydrogen: Tuning Primary and Secondary Coordination Spheres

Jonathan M. Darmon, Simone Raugei, Tianbiao Liu, Elliott B. Hulley, Charles J. Weiss, R. Morris Bullock, and Monte L. Helm*

Center for Molecular Electrocatalysis, Physical Sciences Division, Pacific Northwest National Laboratory, P.O. Box 999, K2-57, Richland, Washington 99352, United States

Supporting Information

ABSTRACT: A series of iron hydride complexes featuring $P^RN^{R'}P^R$ ($P^RN^{R'}P^R = R_2PCH_2N(R')CH_2PR_2$ where R = Ph, R′ = Me; R = Et, R′ = Ph, Bn, Me, ^{t}Bu) and cyclopentadienide (Cp^X = C_5H_4X where X = H, C_5F_4N) ligands has been synthesized; characterized by NMR spectroscopy, X-ray diffraction, and cyclic voltammetry; and examined by quantum chemistry calculations. Each compound was tested for the electrocatalytic oxidation of H_2, and the most active complex, $(Cp^{C_5F_4N})Fe(P^{Et}N^{Me}P^{Et})(H)$, exhibited a turnover frequency of 8.6 s^{-1} at 1 atm of H_2 with an overpotential of 0.41 V, as measured at the potential at half of the catalytic current and using N-methylpyrrolidine as the exogenous base to remove protons. Control complexes that do not contain pendant amine groups were also prepared and characterized, but no catalysis was observed. The rate-limiting steps during catalysis are identified through combined experimental and computational studies as the intramolecular deprotonation of the Fe^{III} hydride by the pendant amine and the subsequent deprotonation by an exogenous base.

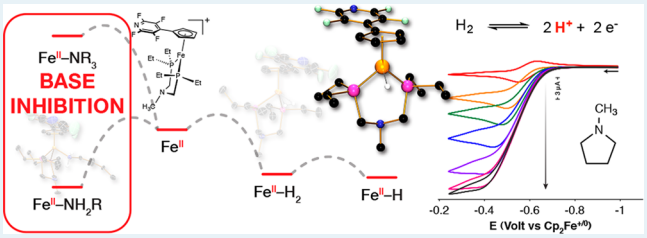

KEYWORDS: *iron, electrocatalyst, hydrogen oxidation, proton relay, diphosphine, piano-stool*

INTRODUCTION

As the world's energy demand increases, one of science's great challenges is the development of technologies that provide inexpensive, readily available, sustainable energy. Harvesting only a fraction of the energy output by the sun, for example, would lessen our dependence on nonrenewable resources (i.e., coal, natural gas, etc.) and decrease our carbon footprint.[1,2] However, temporal and geographic variability dictate the abundance of renewable resources around the world and present a fundamental challenge. One promising solution is to convert renewable energy into chemical bonds, like that in H_2, which can be accessed later through combustion or electrocatalytic processes (Scheme 1).[1] Electrocatalysis, which has the potential to be more efficient than combustion, has generated a growing interest in the scientific community and represents a blossoming area of research.

Current fuel cell technologies to convert the energy in H_2 to electricity rely upon precious metals, particularly platinum, which limits widespread global adoption.[3−5] Their low terrestrial abundance, coupled with increased demand from other industries (i.e., automotive, commodity chemicals, etc.) has resulted in a volatile precious metals market and underscores the need for alternatives that do not utilize scarce elements.[6−8] Iron is an inexpensive, abundant element that has tremendous promise as a replacement for precious metals used in industry.[6,9] More importantly, Nature's [FeFe] hydrogenase is capable of catalytically oxidizing H_2 at a rate of 28 000 s^{-1}, demonstrating iron's potential as a precious metal surrogate for fuel cell applications.[10]

Camara and Rauchfuss reported catalytic oxidation of H_2 by a diiron complex that has a redox-active derivative of ferrocene.[11] Their reactions used a chemical oxidant, and their complex provides a structural model for the [FeFe]-hydrogenase. Sun and co-workers recently reported a [FeFe]-hydrogenase model complex that also oxidizes H_2 at 1 atm and 25 °C.[12] Research in our laboratories has focused on the design of biologically inspired functional models of hydrogenase active sites.[12−15] In particular, we have shown that incorporation of pendant amines can result in substantial improvements in catalytic activity.[16−18] Understanding the precise role of the pendant amine has been a primary focus of our research in developing nickel, cobalt, and iron molecular electrocatalysts for the production and oxidation of H_2.[16−21] For example, the

Scheme 1. Electrochemical Release of Energy from H_2

$$H_2 \rightleftharpoons 2\,H^+ + 2\,e^-$$

$$2\,H^+ + 2\,e^- + {}^1/_2\,O_2 \rightleftharpoons H_2O$$

$$H_2 + {}^1/_2\,O_2 \longrightarrow H_2O + \textit{energy}$$

Received: March 4, 2014
Published: March 7, 2014

   dx.doi.org/10.1021/cs500290w | ACS Catal. 2014, 4, 1246−1260

Scheme 2. An Iron Complex Containing a Pendant Amine Competent for the Heterolytic Cleavage and Formation of the H−H Bond

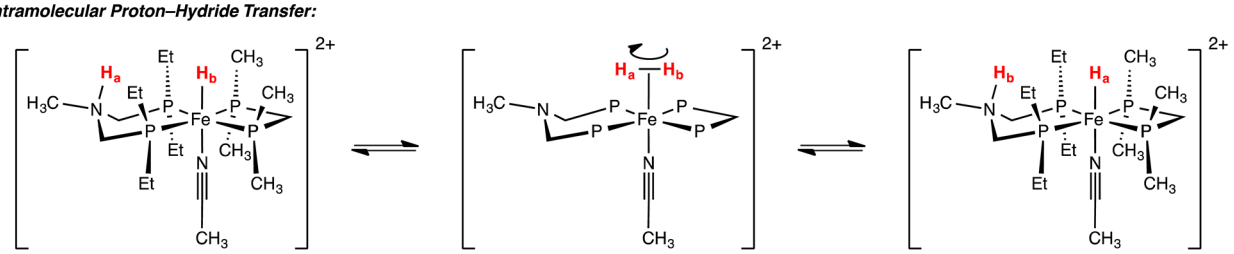

structure of the $[Ni(P^{R}_{2}N^{R'}_{2})_{2}]^{2+}$ ($P^{R}_{2}N^{R'}_{2}$ = $RP(CH_2N(R')CH_2)_2PR$) catalysts for H_2 production/oxidation was developed using an approach that encompassed tuning the first and second coordination spheres around the metal center.[22] The first coordination sphere consists of the ligands that are directly attached to the metal. The second coordination sphere consists of functional groups incorporated into the ligand structure that ideally interact with substrates and not the metal (i.e., Scheme 2). The first coordination sphere influences the properties of the metal center, such as the presence or absence of vacant coordination sites, redox potentials, and electron density. The second coordination sphere allows for control over the delivery of protons to and from the reaction medium to the metal center, particularly through adjusting the basicity of the pendant amines. Careful tuning of the thermodynamics of the metal complexes avoids large activation barriers and both high or low energy intermediates that can hinder catalytic activity. When the coordination spheres are properly optimized, turnover frequencies (TOFs) and overpotentials are vastly improved for the catalytic reactions, emphasizing the importance of their careful design for molecular catalysts.[16−18]

Early efforts applying these principles to develop iron electrocatalysts yielded complexes that demonstrated evidence for rapid heterolytic cleavage and formation of the H−H bond (e.g., Scheme 2).[23,24] These studies ultimately culminated in the synthesis of $(Cp^{C_6F_5})Fe(P^{tBu}_{2}N^{Bn}_{2})(H)$ ($Cp^{C_6F_5}$ = $C_5H_4C_6F_5$; $P^{tBu}_{2}N^{Bn}_{2}$ = $^{t}BuP[CH_2N(Bn)CH_2]_2P^{t}Bu$), the first example of a homogeneous iron electrocatalyst for the oxidation of H_2.[19] A turnover frequency of 2.0 s^{-1} under 1 atm H_2 at 22 °C and an overpotential of 0.16 V (as measured at the potential at half of the catalytic current, $E_{cat/2}$) was observed using *N*-methylpyrrolidine as the exogenous base.

Herein, we describe the synthesis and study of a new generation of iron electrocatalysts for the oxidation of H_2 containing $P^{R}N^{R'}P^{R}$ ($P^{R}N^{R'}P^{R}$ = $R_2PCH_2N(R')CH_2PR_2$ where R = Ph, R′ = Me; R = Et, R′ = Ph, Bn, Me, ^{t}Bu) and Cp^{X} (Cp^{X} = C_5H_4X where X = H, C_5F_4N) ligands. Substituents on the cyclopentadienyl and $P^{R}N^{R'}P^{R}$ ligands were selected to probe the effect of the pendant amine (R′), the impact of the steric environment (R), and the acidity of the hydride and dihydrogen ligands on iron. In particular, the $Cp^{C_5F_4N}$ ligand was chosen to reduce the electron donating ability of the Cp^{X} ligand compared with Cp^{H} and $Cp^{C_6F_5}$. Because coordination of exogenous base inhibits H_2 oxidation for the $(Cp^{X})Fe(P^{R}_{2}N^{R'}_{2})(H)$ family of compounds, we hypothesized that $P^{R}N^{R'}P^{R}$ ligands would provide a greater degree of steric protection to the metal center as a result of their larger phosphorus−metal−phosphorus bite angles and would therefore result in electrocatalysts with higher activities.[19,24] Previous work with Ni electrocatalysts for H_2 oxidation have demonstrated that the pendant amines in $P^{R}N^{R'}P^{R}$ metal complexes are positioned less ideally for heterolytic cleavage compared with the $P^{R}_{2}N^{R'}_{2}$ ligands.[25,26] The instability of Ni^{II}−H_2 complexes requires precisely positioned pendant amines for fast heterolytic cleavage of H_2; however, we hypothesized that the stability of Fe^{II}−H_2 adducts would overcome the need for precise positioning of the pendant amines.[23,27] The new family of cyclopentadienyl iron complexes features $P^{R}N^{R'}P^{R}$ ligands that explore the effect of the phosphorus, nitrogen, and cyclopentadienyl substituents on the electrocatalytic oxidation of dihydrogen.

RESULTS AND DISCUSSION

Synthesis of Iron Hydride Complexes with PNP Ligands. A family of iron complexes incorporating $P^{R}N^{R'}P^{R}$ ($P^{R}N^{R'}P^{R}$ = $R_2PCH_2N(R')CH_2PR_2$ where R = Ph, R′ = Me; R = Et, R′ = Ph, Bn, Me, ^{t}Bu) ligands was prepared using a method similar to that used for $(Cp^{C_6F_5})Fe(P^{tBu}_{2}N^{Bn}_{2})(H)$.[24] Synthesis used of the diphosphine iron dichloride complexes, $(P^{R}N^{R'}P^{R})FeCl_2$, was accomplished by stirring the diphosphine with $FeCl_2$ in THF for 12−24 h (eq 1). Each of the complexes

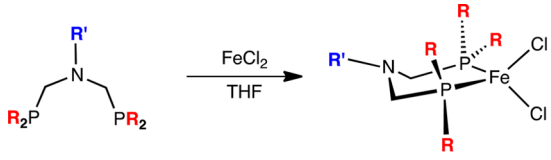

(1)

R = Ph, R' = CH_3 — $(P^{Ph}N^{Me}P^{Ph})FeCl_2$
R = Et, R' = CH_3 — $(P^{Et}N^{Me}P^{Et})FeCl_2$
R = Et, R' = Ph — $(P^{Et}N^{Ph}P^{Et})FeCl_2$
R = Et, R' = Bn — $(P^{Et}N^{Bn}P^{Et})FeCl_2$
R = Et, R' = ^{t}Bu — $(P^{Et}N^{tBu}P^{Et})FeCl_2$

was isolated in high yield (95−98%). The ^{1}H NMR spectra of the complexes exhibit the number of paramagnetically broadened resonances expected for C_{2v}-symmetric molecules over the range of −10 to 140 ppm. We presume that the $(P^{R}N^{R'}P^{R})FeCl_2$ complexes are monomeric and have a tetrahedral geometry, as established by X-ray crystallography of an analogous complex, $(P^{tBu}_{2}N^{Bn}_{2})FeCl_2$.[19]

Addition of 1 equivalent of $NaCp^{X}$ (Cp^{X} = C_5H_4X where X = H, C_5F_4N) to a THF slurry of $(P^{R}N^{R'}P^{R})FeCl_2$ at −35 °C furnished the $(Cp^{X})Fe(P^{R}N^{R'}P^{R})(Cl)$ complexes following filtration and recrystallization from diethyl ether (eq 2). With the exception of $(Cp^{H})Fe(P^{Ph}N^{Me}P^{Ph})(Cl)$, each compound was isolated as a diamagnetic solid in good yield (86−95%) and

dx.doi.org/10.1021/cs500290w | ACS Catal. 2014, 4, 1246−1260

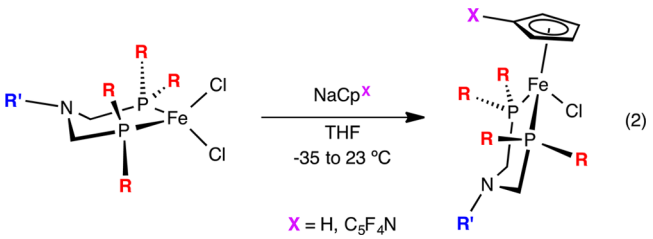

(2)

thoroughly characterized. Given the low yield (23%) of $(Cp^{H})Fe(P^{Ph}N^{Me}P^{Ph})(Cl)$ using the above route, an alternative method entailing the photolysis of $(Cp^{H})Fe(CO)_2Cl$ in the presence of $P^{Ph}N^{Me}P^{Ph}$ was developed, providing the complex in 70% yield. In each case, the ^1H NMR spectra exhibit the number of resonances consistent with a diamagnetic C_{2v} symmetric molecule, and a single $^{31}P\{^1H\}$ NMR resonance is observed between 42 and 51 ppm.

Stirring each $(Cp^{X})Fe(P^{R}N^{R'}P^{R})(Cl)$ complex in ethanol with excess $NaBH_4$ resulted in conversion to the corresponding iron hydride, $(Cp^{X})Fe(P^{R}N^{R'}P^{R})(H)$ (eq 3). Filtration and

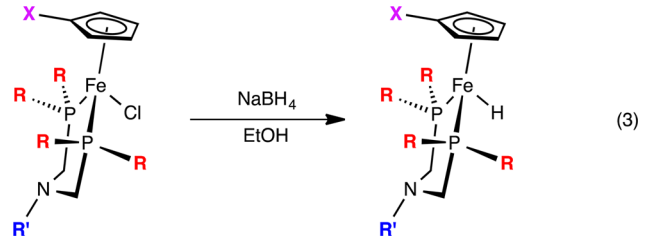

(3)

recrystallization from pentane or diethyl ether at −35 °C furnished the complexes as diamagnetic, crystalline solids in good yield (86−97%). Each of the iron hydride complexes was characterized by NMR spectroscopy and cyclic voltammetry. The iron hydride resonances in the ^1H NMR spectra are observed between −15 and −17.5 ppm as triplets ($^2J_{PH}$ = 70−73 Hz), arising from coupling to the two equivalent phosphine atoms. Correspondingly, the ^{31}P NMR spectra exhibit a doublet resonance between 65 and 75 ppm.

The $(Cp^{C_5F_4N})Fe(P^{Et}N^{Bn}P^{Et})(Cl)$, $(Cp^{C_5F_4N})Fe(P^{Ph}N^{Me}P^{Ph})(H)$, and $(Cp^{C_5F_4N})Fe(P^{Et}N^{Me}P^{Et})(H)$ complexes were further characterized by single-crystal X-ray diffraction. Representations of the solid-state structures are presented in Figure 1, and metrical parameters are reported in Table 1. Each complex adopts a three-legged piano-stool geometry, where the six-membered ring made up by the PNP backbone and the iron

Table 1. Bond Distances (Å) and Angles (deg) for $(Cp^{C_5F_4N})Fe(P^{Et}N^{Bn}P^{Et})(Cl)$, $(Cp^{C_5F_4N})Fe(P^{Ph}N^{Me}P^{Ph})(H)$, and $(Cp^{C_5F_4N})Fe(P^{Et}N^{Me}P^{Et})(H)$

	$(Cp^{C_5F_4N})Fe(P^{Et}N^{Bn}P^{Et})(Cl)$	$(Cp^{C_5F_4N})Fe(P^{Ph}N^{Me}P^{Ph})(H)$	$(Cp^{C_5F_4N})Fe(P^{Et}N^{Me}P^{Et})(H)$
Fe(1)−P(1)	2.2014(5)	2.1347(5)	2.1447(4)
Fe(1)−P(2)	2.1980(5)	2.1227(5)	2.1391(4)
P(1)−Fe(1)−P(2)	92.204(18)	93.683(19)	92.031(14)
Cp^{cent}−Fe(1)−P(1)	126.22	131.04	131.81
Cp^{cent}−Fe(1)−P(2)	125.22	127.27	130.38

atom adopts a chair conformation. In one example, $(Cp^{C_5F_4N})$-$Fe(P^{Ph}N^{Me}P^{Ph})(H)$, a $\pi-\pi$ stacking interaction exists between the tetrafluoropyridyl substituent of the cyclopentadienide and one of the phenyl substituents (distance between centroids = 3.467 Å) in the solid state. Each of the complexes exhibits a P−Fe−P bite angle of 92−94°, which is approximately 10° wider than the iron complexes previously characterized with $P^{R}{}_2N^{R'}{}_2$ ligands.[19,24]

Synthesis of a Dihydrogen Complex. Stirring a fluorobenzene slurry of $(Cp^{C_5F_4N})Fe(P^{Et}N^{Me}P^{Et})(Cl)$ in the presence of 1 equivalent of $NaBAr^{F}{}_4$ [Ar^{F} = 3,5-bis-(trifluoromethyl)phenyl] under 1 atm H_2 furnished the H_2 adduct, $[(Cp^{C_5F_4N})Fe(P^{Et}N^{Me}P^{Et})(H_2)]^+$, in high yield (86%) as an orange-yellow crystalline solid following filtration and precipitation with pentane. The complex exhibits a singlet in the $^{31}P\{^1H\}$ NMR spectrum at 51.1 ppm and a broad resonance ($\nu_{1/2}$ = 72 Hz) at −13.7 ppm assigned to the H_2 ligand in the ^1H NMR spectrum. These spectral features are consistent with formation of a dihydrogen adduct analogous to the previously reported $P^{R}{}_2N^{R'}{}_2$ complexes.[19,24] X-ray quality crystals were obtained from layering a saturated fluorobenzene solution of the compound with hexanes. A representation of the solid-state structure is presented in Figure 2, and metrical parameters are reported in Table 2. The hydrogen atoms of the H_2 molecule were located in the difference map and restrained to be equidistant from the iron atom. The geometry about the iron center is not significantly different from the neutral complexes described above. The six-membered ring formed between the $P^{Et}N^{Me}P^{Et}$ ligand and the Fe atom crystallized in a chair conformation; however, previous studies have shown that chair−boat isomerization is facile in solution.[28]

Electrochemistry of the Iron Hydride Complexes. Cyclic voltammetry experiments on the $(Cp^{X})Fe$-

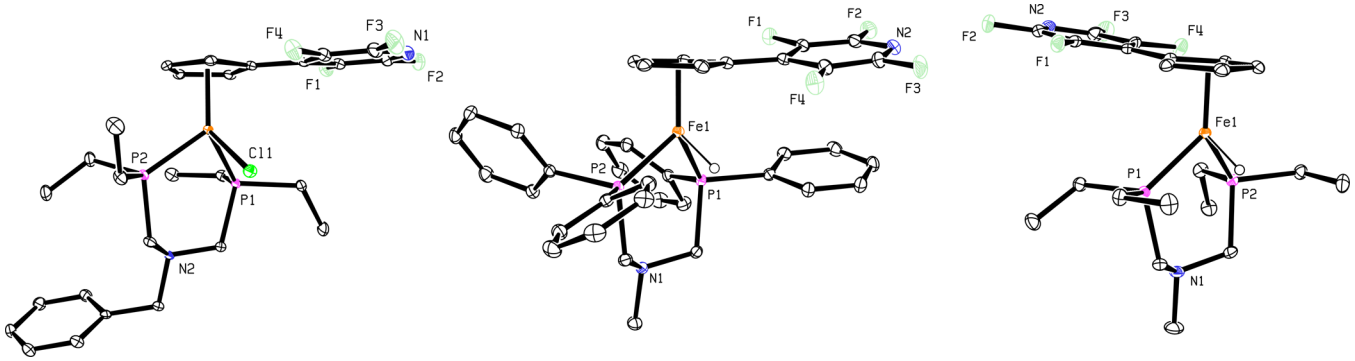

Figure 1. Solid-state structure of $(Cp^{C_5F_4N})Fe(P^{Et}N^{Bn}P^{Et})(Cl)$ (left), $(Cp^{C_5F_4N})Fe(P^{Ph}N^{Me}P^{Ph})(H)$ (middle), and $(Cp^{C_5F_4N})Fe(P^{Et}N^{Me}P^{Et})(H)$ (right) at 30% probability ellipsoids. All hydrogen atoms, with the exception of the Fe−H, have been omitted for clarity.

dx.doi.org/10.1021/cs500290w | ACS Catal. 2014, 4, 1246−1260

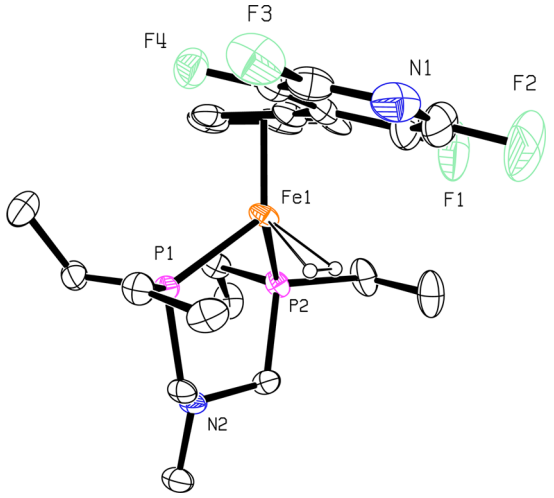

Figure 2. Solid-state structure of $[(Cp^{C_5F_4N})Fe(P^{Et}N^{Me}P^{Et})(H_2)]^+$ at 30% probability ellipsoids. All hydrogen atoms, with the exception of H_2, and the $BAr^F{}_4^-$ anion have been omitted for clarity.

Table 2. Bond Distances (Å) and Angles (deg) for $[(Cp^{C_5F_4N})Fe(P^{Et}N^{Me}P^{Et})(H_2)]^+$

$[(Cp^{C_5F_4N})Fe(P^{Et}N^{Me}P^{Et})(H_2)]^+$	
Fe(1)–P(1)	2.1884(10)
Fe(1)–P(2)	2.1952(11)
P(1)–Fe(1)–P(2)	90.47(4)
Cp^{cent}–Fe(1)–P(1)	124.47
Cp^{cent}–Fe(1)–P(2)	125.11

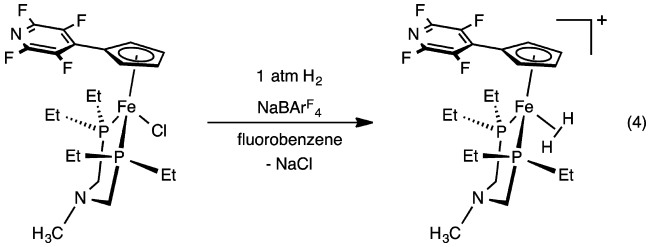

$(P^RN^{R'}P^R)(H)$ compounds were performed in a 0.1 M $[^nBu_4N][B(C_6F_5)_4]$ fluorobenzene solution, and the data are summarized in Table 3. Each complex exhibits a reversible or quasi-reversible one-electron voltammogram corresponding to the $Fe^{II/III}$ couple at 50 mV/s (e.g., Figure 3, see Supporting Information (SI), Figure S1). Plots of the anodic peak current (i_p) versus the square root of the scan rate are linear, indicating

Table 3. Electrochemical Data for the $(Cp^X)Fe(P^RN^{R'}P^R)(H)^{+/0}$ Couple[a]

compd	$E_{1/2}$ (V vs $Cp_2Fe^{+/0}$)[b]	ΔE_p (mV)[c]	$i_{cathodic}/i_{anodic}$
$(Cp^H)Fe(P^{Ph}N^{Me}P^{Ph})(H)$	−0.67	80	1.0
$(Cp^{C_5F_4N})Fe(P^{Ph}N^{Me}P^{Ph})(H)$	−0.40	84	0.6
$(Cp^{C_5F_4N})Fe(P^{Et}N^{Ph}P^{Et})(H)$	−0.53	82	1.0
$(Cp^{C_5F_4N})Fe(P^{Et}N^{Bn}P^{Et})(H)$	−0.57	75	0.9
$(Cp^{C_5F_4N})Fe(P^{Et}N^{Me}P^{Et})(H)$	−0.58	85	0.8
$(Cp^{C_5F_4N})Fe(P^{Et}N^{tBu}P^{Et})(H)$	−0.60	77	0.9

[a]Conditions: 1 mM [Fe], 0.1 M $[^nBu_4N][B(C_6F_5)_4]$, fluorobenzene solution. Potentials are referenced to $Cp_2Fe^{+/0}$. [b]Average values over scan rates of 0.02−1.00 V/s. [c]Scan rate of 0.05 V/s.

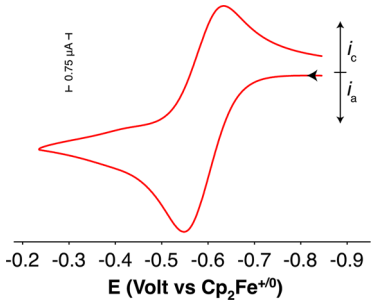

Figure 3. Reversibility of the $Fe^{II/III}$ couple for $(Cp^{C_5F_4N})Fe(P^{Et}N^{Me}P^{Et})(H)$. Conditions: 1 mM [Fe], 0.1 M $[^nBu_4N][B(C_6F_5)_4]$, fluorobenzene solution, 50 mV/s. Potentials are referenced to $Cp_2Fe^{+/0}$.

a diffusion-controlled redox process. With increasing scan rate, the redox event for each complex becomes increasingly reversible (see SI, Figure S2). In contrast to the $Fe^{II/III}$ couple of the $(Cp^X)Fe(P^RN^{R'}P^R)(H)$ compounds, the $(Cp^X)Fe(P^R{}_2N^{R'}{}_2)(H)$ analogs exhibit irreversible $Fe^{II/III}$ couples at slow scan rates (<100 mV/s) attributed to intra- and intermolecular proton transfers, resulting in H_2 elimination (Scheme 3).[19,24] A similar process is thought to be occurring in the $(Cp^X)Fe(P^RN^{R'}P^R)(H)$ family of complexes; however, at significantly slower rates than the $(Cp^X)Fe(P^R{}_2N^{R'}{}_2)(H)$ analogs, resulting in the greater relative reversibility of the $Fe^{II/III}$ couple.

The $Fe^{II/III}$ couple for the $(Cp^X)Fe(P^RN^{R'}P^R)(H)$ complexes is strongly influenced by the substituents on the cyclopentadienyl and phosphine ligands. Introduction of the tetrafluoropyridyl substituent to the cyclopentadienyl ligand in $(Cp^{C_5F_4N})Fe(P^{Ph}N^{Me}P^{Ph})(H)$ results in a potential shift of +0.27 V as compared with $(Cp^H)Fe(P^{Ph}N^{Me}P^{Ph})(H)$. Substitution of the phenyl substituents on phosphorus in $(Cp^{C_5F_4N})Fe(P^{Ph}N^{Me}P^{Ph})(H)$ to the electron-donating alkyl groups in $(Cp^{C_5F_4N})Fe(P^{Et}N^{Me}P^{Et})(H)$ produces a −0.18 V shift. The influence of changing R′ on the pendant amine in the $P^RN^{R'}P^R$ ligands results in a +0.07 V shift from R′ = ^{t}Bu to R′ = Ph.

Electrocatalytic Oxidation of Dihydrogen. Each of the new $(Cp^X)Fe(P^RN^{R'}P^R)(H)$ complexes was evaluated for the electrocatalytic oxidation of H_2. Conditions for catalytic electrochemical measurements employed a 1 mM solution of the iron complex dissolved in a 0.1 M $[^nBu_4N][B(C_6F_5)_4]$ fluorobenzene solution, 1 atm of H_2, and subsequent additions of *N*-methylpyrrolidine as the exogenous base to remove protons. Catalytic oxidation of H_2 was identified by an increase in the anodic peak current near the $Fe^{III/II}$ couple upon addition of the exogenous base (Figure 4). The catalytic current was measured at the point where the catalytic wave first plateaus (Figure 4, i_{cat}). The half-wave potential for the catalytic process, $E_{cat/2}$, was defined at half the catalytic current (Figure 4, $E_{cat/2}$). Turnover frequencies (k_{obs}, eq 5) were determined from the ratio of i_{cat}/i_p using eq 6, where n is the number of electrons (2 for H_2 oxidation), R is the gas constant (8.314 J K^{-1} mol^{-1}), F is Faraday's constant (9.65×10^4 C/mol), T is the temperature (298 K), and υ is the scan rate in V/s.[29−32] The overpotential was determined by the method recently reported by Roberts and Bullock that is based on experimental open circuit measurements to determine the thermodynamic potential for

Scheme 3. Rapid Intramolecular Proton Transfer of $(Cp^{C_5F_5})Fe(P^{tBu}{}_2N^{Bn}{}_2)(H)$, Resulting in Electrochemical Irreversibility at Slow Scan Rates

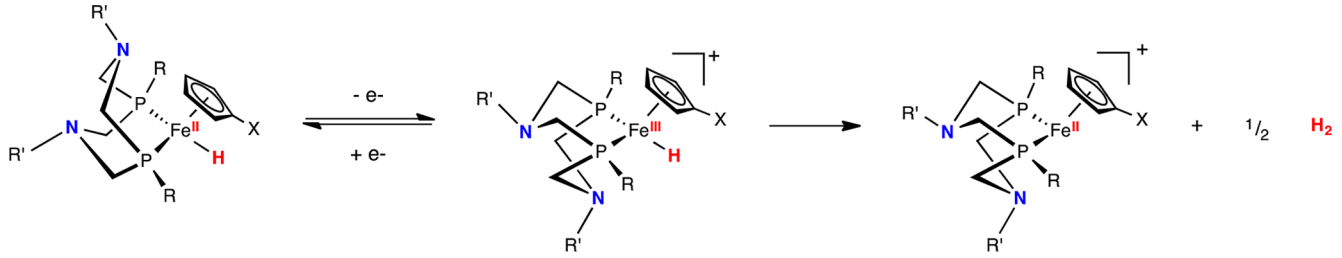

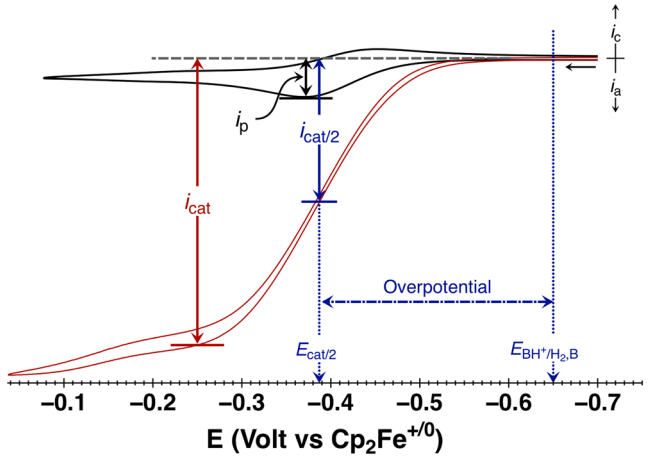

Figure 4. (a) Cyclic voltammograms of a fluorobenzene solution of $(Cp^{C_5F_4N})Fe(P^{Ph}N^{Me}P^{Ph})(H)$ (black) and subsequent current enhancement upon addition of 77 mM *N*-methylpyrrolidine (red). Conditions: 1 mM [Fe], 0.1 M $[^nBu_4N][B(C_6F_5)_4]$, 1 atm H_2, 50 mV/s. Potentials are referenced to $Cp_2Fe^{+/0}$.

proton reduction/H_2 oxidation at a platinum electrode in solutions identical to those used to determine catalytic rates (Figure 4).[33,34] The electrocatalytic oxidation of H_2 with $(Cp^{C_5F_4N})Fe(P^{Et}N^{Me}P^{Et})(H)$ was confirmed through bulk electrolysis, and average current efficiencies greater than 90% were determined by ^1H NMR spectroscopy (see the Experimental Section).

$$\text{rate} = k_{obs}[\text{cat}]^x \qquad (k_{obs} = \text{turnover frequency}) \tag{5}$$

$$\frac{i_{cat}}{i_p} = \frac{n}{0.4463}\sqrt{\frac{RTk_{obs}}{F\upsilon}} \tag{6}$$

Of the six complexes reported in this study, $(Cp^{C_5F_4N})Fe(P^{Ph}N^{Me}P^{Ph})(H)$ and $(Cp^{C_5F_4N})Fe(P^{Et}N^{Me}P^{Et})(H)$ are shown to electrocatalytically oxidize H_2 at measurable rates (Figure 5) using cyclic voltammetry (as defined by $i_{cat}/i_p > 4$). Turnover frequencies of 6.7 s^{-1} and 8.6 s^{-1} under 1 atm of H_2 were determined for $(Cp^{C_5F_4N})Fe(P^{Ph}N^{Me}P^{Ph})(H)$ and $(Cp^{C_5F_4N})Fe(P^{Et}N^{Me}P^{Et})(H)$, respectively (Table 4). The rate law for the oxidation of H_2 by these catalysts is shown in eq 7. In the presence of 0.1 M *N*-methylpyrrolidine, the i_{cat} observed in catalysis by $(Cp^{C_5F_4N})Fe(P^{Et}N^{Me}P^{Et})(H)$ increases linearly as a function of catalyst concentration between 0.3 and 1.0 mM, indicating the reaction is first-order in catalyst concentration (i.e., eq 5, $x = 1$; see SI, Figure S3). For both complexes, the catalytic current becomes independent of both base concentration and scan rate above 0.1 M *N*-methylpyrrolidine and a scan rate of ≥0.020 V/s (i.e., $y = 0$, eq 8). Under these conditions, the catalytic process is pseudo-zero-order with respect to base concentration, so the turnover frequency (k_{obs}) depends only on the H_2 pressure (i.e., eq 9).

$$\text{rate} = k[\text{cat}]^x[\text{base}]^y P_{H_2}{}^z \tag{7}$$

$$k_{obs} = k[\text{base}]^y P_{H_2}{}^z \tag{8}$$

$$k_{obs} = k \cdot P_{H_2}{}^z \tag{9}$$

Mechanistic Discussion. A CECE mechanism is proposed for H_2 oxidation by $(Cp^{C_5F_4N})Fe(P^RN^{Me}P^R)(H)$ (R = Et, Ph; Figure 6), consisting of alternating chemical (C) and electrochemical (E) steps on the basis of experimental and computational results as well as the previously reported complexes that incorporate the $P^R{}_2N^{R'}{}_2$ ligand framework.[19,24] Beginning the catalytic cycle, formation of the 16-electron $[(Cp^{C_5F_4N})Fe(P^RN^{Me}P^R)]^+$ complexes is followed by addition of H_2, leading to an H_2 adduct (Figure 6, step 1), which may be in exchange with the heterolytically cleaved proton hydride species (Figure 6, step 2).[24,35] In the presence of an exogenous base, the proton hydride species is deprotonated (CECE, Figure 6, step 3) giving the Fe^{II} hydride complex. Oxidation of the Fe^{II} hydride to an Fe^{III} hydride (CECE, Figure 6, step 4) lowers the pK_a of the complex and results in either intramolecular proton transfer from the iron to the pendant amine (Figure 6, step 5a), followed by intermolecular deprotonation by the exogenous base (CECE, Figure 6, step 5b), or direct deprotonation of the Fe^{III} hydride by the exogenous base (Figure 6, step 5c). The resulting 17-electron Fe^I complex undergoes a second one-electron oxidation (CECE, Figure 6, step 6), yielding the starting 16-electron Fe^{II} species, and completing the catalytic cycle. Experimental and computational results to support this mechanism are presented below.

Although dihydrogen addition to the 16-electron $[(Cp^{C_5F_4N})Fe(P^RN^{Me}P^R)]^+$ complexes (Figure 6, step 1) is thought to be facile, previously reported mechanistic studies of H_2 oxidation by the $(Cp^X)Fe(P^R{}_2N^{R'}{}_2)(H)$ family of compounds revealed competitive binding of the exogenous base (Figure 6, step 7) can inhibit catalysis.[19,24] In the presence of $^nBuNH_2$, which has a basicity similar to that of *N*-methylpyrrolidine, H_2 oxidation is not observed with $(Cp^{C_5F_4N})Fe(P^RN^{Me}P^R)(H)$ (R = Et, Ph) (see SI, Figure S4). Indeed, addition of $^nBuNH_2$ to the unsaturated species, $[(Cp^{C_5F_4N})Fe(P^{Et}N^{Me}P^{Et})]^+$, led to isolation and full characterization of the amine bound $[(Cp^{C_5F_4N})Fe(P^{Et}N^{Me}P^{Et})(NH_2{}^nBu)]^+$ complex (Figure 7, see SI for metrical parameters). Computational results, however, indicate formation of an amine complex with *N*-methylpyrrolidine is not favored, likely because of steric clashes between the pyrrolidine ring and the other ligands of the Fe complex (vide infra). In the

dx.doi.org/10.1021/cs500290w | ACS Catal. 2014, 4, 1246−1260

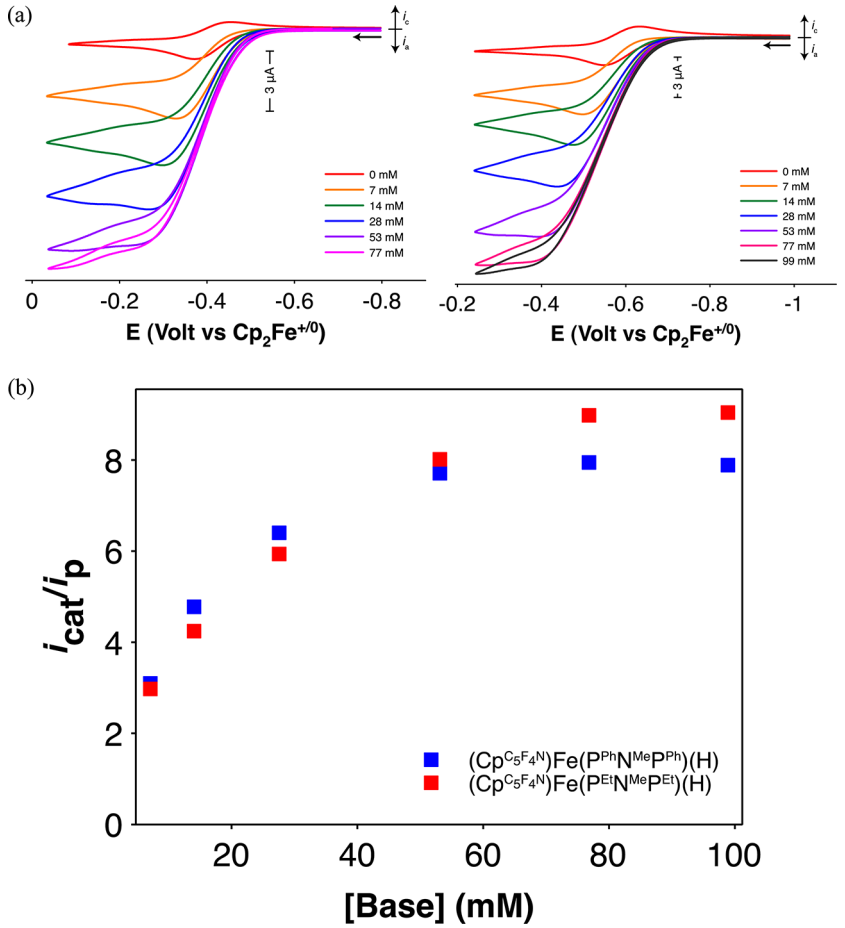

Figure 5. (a) Cyclic voltammograms of a fluorobenzene solution of $(Cp^{C_5F_4N})Fe(P^{Ph}N^{Me}P^{Ph})(H)$ (left) and $(Cp^{C_5F_4N})Fe(P^{Et}N^{Me}P^{Et})(H)$ (right) upon addition of *N*-methylpyrrolidine under 1 atm H_2 at 22 °C. (b) Current enhancement as a function of the concentration of *N*-methylpyrrolidine. Conditions: 1 mM [Fe], 0.1 M $[^nBu_4N][B(C_6F_5)_4]$, 1 atm H_2, 50 mV/s. Potentials are referenced to $Cp_2Fe^{+/0}$. Values of i_{cat}/i_p were corrected for dilution using the internal reference.

Table 4. Turnover Frequencies (TOF) and Overpotentials (in parentheses) for Electrocatalytic Oxidation of H_2

compd	TOF (overpotential)[a]
$(Cp^H)Fe(P^{Ph}N^{Me}P^{Ph})(H)$	NC[b]
$(Cp^{C_5F_4N})Fe(P^{Ph}N^{Me}P^{Ph})(H)$	6.7 s^{-1} (0.56 V)
$(Cp^{C_5F_4N})Fe(P^{Et}N^{Ph}P^{Et})(H)$	NC
$(Cp^{C_5F_4N})Fe(P^{Et}N^{Bn}P^{Et})(H)$	slow[c]
$(Cp^{C_5F_4N})Fe(P^{Et}N^{Me}P^{Et})(H)$	8.6 s^{-1} (0.41 V)
$(Cp^{C_5F_4N})Fe(P^{Et}N^{tBu}P^{Et})(H)$	slow[c]

[a]Conditions: 1 mM [Fe], 0.1 M $[^nBu_4N][B(C_6F_5)_4]$, fluorobenzene solution, 50 mV/s. Potentials are referenced to $Cp_2Fe^{+/0}$. [b]NC = No appreciable current enhancement was observed, indicating the compound does not facilitate catalytic oxidation of H_2. [c]TOF < 1.7 s^{-1}.

case of $^nBuNH_2$, favorable hydrogen bonding between the N–H bond of the coordinated amine and the pendant amine is observed in the solid-state structure (N(1)···N(2) = 2.876 Å) and is reproduced computationally. This interaction provides stability for the binding of $^nBuNH_2$ to the $[(Cp^{C_5F_4N})Fe(P^{Et}N^{Me}P^{Et})]^+$ complex and has been computationally estimated to be ~2 kcal/mol.

In an attempt to disfavor binding of a base to the 16-electron Fe^{II} complexes, *N*,*N*-diisopropylethylamine (Hünig's base), a more sterically encumbered base with a pK_a similar to that of *N*-methylpyrrolidine, was examined. Rather than leading to increased rates of H_2 oxidation, the rate of catalysis is much slower, exhibiting current enhancements with i_{cat}/i_p values of <2 (see SI, Figure S5). The difference in activity observed with the different bases, *N*-methylpyrrolidine and *N*,*N*-diisopropylethylamine, is attributed to an increase in the barrier for deprotonation resulting from the steric environment around the amine and cannot be accounted for by pK_a matching or a difference in the base binding to the 16-electron species.[19]

The dihydrogen ligand in the $[(Cp^{C_5F_4N})Fe(P^{Et}N^{R}P^{Et})(H_2)]^+$ complexes is thought to undergo rapid, reversible heterolytic cleavage resulting in a dynamic equilibrium with the proton hydride $[(Cp^{C_5F_4N})Fe(H)(P^{Et}N^{R}(H)P^{Et})]^+$ species (Figure 6, step 2).[24] This process can be exceedingly facile in suitably energy-matched systems, where the proton acceptor ability of the amine and the hydride acceptor ability of the metal are adjusted so that the free energy for heterolytic cleavage of H_2 is very low. We recently reported related Fe and Mn complexes with pendant amines in which the barrier to proton/hydride exchange was found to be <6.8 kcal mol^{-1} at low temperatures.[35,36] Computational data indicate that this system, much like the previously reported $(Cp^H)Fe(P^R{}_2N^{R'}{}_2)$ compounds, is likely similarly energy-matched (Figure 8).[19] After H_2 addition, deprotonation of the $[(Cp^{C_5F_4N})Fe(P^RN^{Me}P^R)(H_2)]^+$ (R = Ph, Et) complex leads to formation of the Fe^{II} hydride (Figure 6, step 3). To further illustrate the formation of the Fe^{II} hydride in the catalytic pathway, 5 equivalents of *N*-methylpyrrolidine was

dx.doi.org/10.1021/cs500290w | ACS Catal. 2014, 4, 1246–1260

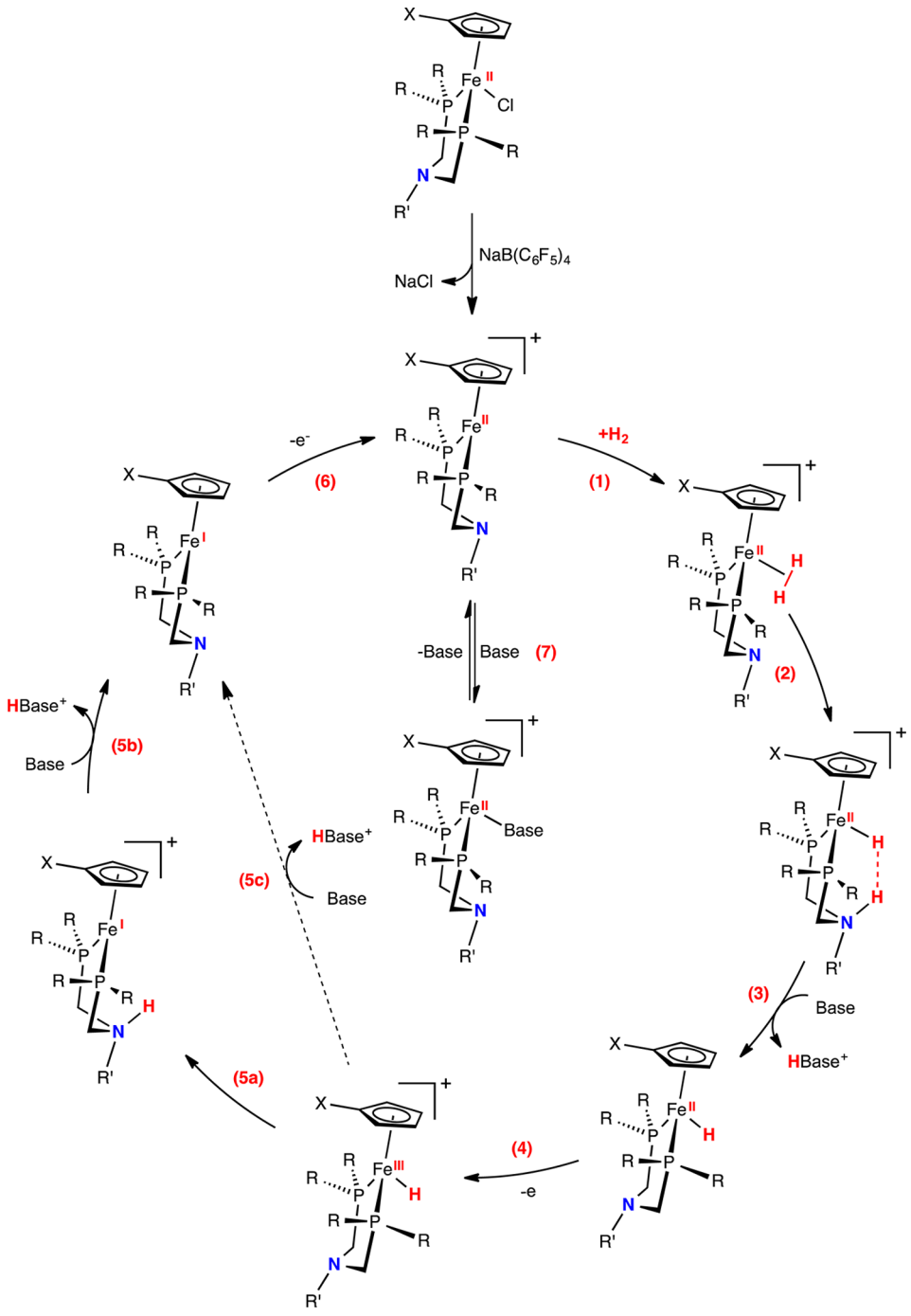

Figure 6. Proposed mechanism for the electrocatalytic oxidation of H_2 by $[(Cp^X)Fe(P^RN^{R'}P^R)]^+$ (X = C_5F_4N; R = Et, Ph; R′ = CH_3).

added to the dihydrogen adduct, $[(Cp^{C_5F_4N})Fe(P^{Et}N^{Me}P^{Et})(H_2)]^+$, resulting in complete conversion to the iron hydride species, $(Cp^{C_5F_4N})Fe(P^{Et}N^{Me}P^{Et})(H)$, as determined by NMR spectroscopy. The complete free energy landscape from the 16-electron Fe^{II} complex through formation of the Fe^{II} hydride is presented in Figure 8, illustrating the initial steps of the catalytic process are suitably energy-matched and likely not rate-limiting.

The acidity of the Fe^{II} hydride is too low for intramolecular deprotonation by either the pendant amine or the exogenous base; as a result, electrochemical oxidation to the Fe^{III} hydride (Figure 6, step 4) must occur for catalysis to proceed. Oxidation of metal hydrides to produce radical cations $MH^{+\bullet}$ is known to lead to large increases in acidity.[37−40] For example, the pK_a of $HCo(dppe)_2$ in MeCN is 14 pK_a units greater than that of $[HCo(dppe)_2]^+$. The catalytic peak current is observed near the $Fe^{II/III}$ hydride couple, further supporting this hypothesis. After oxidation, deprotonation of the Fe^{III} hydride can occur via two possible pathways (Figure 6, step 5). The first pathway represents an intramolecular proton transfer from the Fe^{III} hydride to the pendant amine, forming a Fe^{I} species with a protonated pendant amine (Figure 6, step 5a). This complex can then be deprotonated by the exogenous base, forming the Fe^{I} 17-electron species (Figure 6, step 5b). Alternatively, the Fe^{III} hydride might be deprotonated directly by the exogenous base, forming the same Fe^{I} 17-electron species (Figure 6, step

dx.doi.org/10.1021/cs500290w | ACS Catal. 2014, 4, 1246−1260

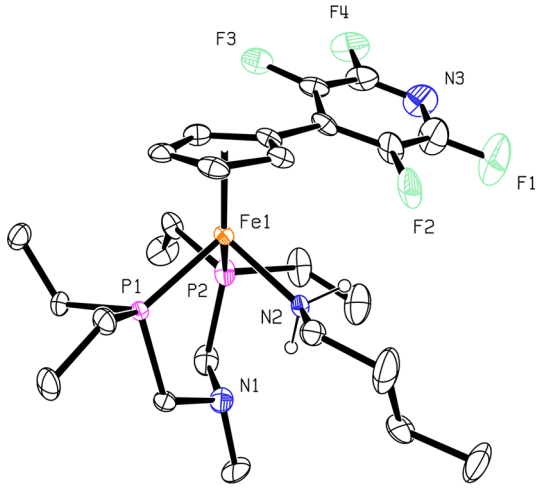

Figure 7. Solid-state structure of $[(Cp^{C_5F_4N})Fe(P^{Et}N^{Me}P^{Et})(NH_2{}^nBu)]^+$ at 30% probability ellipsoids. All hydrogen atoms, with the exception the amine hydrogens, and the $BAr^F{}_4$ counteranion have been omitted for clarity.

5c). Oxidation of the Fe^I 17-electron species occurs negative of the $Fe^{II/III}$ redox couple, resulting in immediate oxidation to the Fe^{II} 16-electron species, completing the catalytic cycle (Figure 6, step 6).

The two possible pathways for deprotonation of the Fe^{III} hydride were explored computationally for three complexes: $[(Cp^{C_5F_4N})Fe(P^{Et}N^{Me}P^{Et})(H)]^+$, $[(Cp^{C_5F_4N})Fe(P^{Ph}N^{Me}P^{Ph})(H)]^+$, and $[(Cp^{H})Fe(P^{Ph}N^{Me}P^{Ph})(H)]^+$ (see SI, Figure S6). Computational results indicate that protonated pendant amines are about 7 (R = Et) and 6 (R = Ph) pK_a units more acidic than the Fe^{III} hydride, which makes the intramolecular proton transfer from the metal center to the pendant amine thermodynamically unfavorable (Figure 6, step 5a). However, although the pK_a's of the Fe^{III} hydride species match reasonably well with the pK_a of protonated *N*-methylpyrrolidine, further computations on $[(Cp^{C_5F_4N})Fe(P^{Et}N^{Me}P^{Et})(H)]^+$ show that a significant energy penalty is required to distort the complex to accommodate the exogenous base in the hydride intermediate (Figure 9). The energy required to distort the two complexes (the Fe^{III} hydride and the Fe^I complex with a protonated pendant amine) are +16.3 and +3.3 kcal/mol, respectively. Therefore, even if the Fe^{III} hydride were more acidic than the protonated pendant amine, the steric environment precludes direct deprotonation by the exogenous base in each of the examples studied.

Additional electrochemical studies conducted on the $(Cp^X)Fe(P^R{}_2N^{R'}{}_2)(H)$ family indicate that intramolecular proton movement, followed by deprotonation of the pendant amine by the exogenous base is the likely route during catalysis. The pseudo-first-order rate constant for this process (Figure 6, steps 4−6) was estimated by examining the reversibility of the $Fe^{II/III}$ couple of the Fe^{II} hydride complexes in the presence of *N*-methylpyrrolidine (and the absence of H_2) as a function of scan rate and base concentration, and the results are summarized in Table 5 (see the SI for a detailed description of the electrochemical procedure). In the case of $[(Cp^{C_5F_4N})Fe(P^RN^{Me}P^R)(H)]^+$ (R = Ph, Et), the pseudo-first-order rate constants were estimated to be >25 s^{-1} at 10 and 50 mM *N*-methylpyrrolidine, respectively. The larger pseudo-first-order rate constant of $[(Cp^{C_5F_4N})Fe(P^{Ph}N^{Me}P^{Ph})(H)]^+$ at lower concentrations of *N*-methylpyrrolidine is attributed to the differences in the pK_a of the Fe^{III} hydrides. The more acidic $[(Cp^{C_5F_4N})Fe(P^{Ph}N^{Me}P^{Ph})(H)]^+$ complex supports a more rapid deprotonation of the hydride. However, these data do not allow us to distinguish between the intramolecular or direct deprotonation pathways for the Fe^{III} hydride.

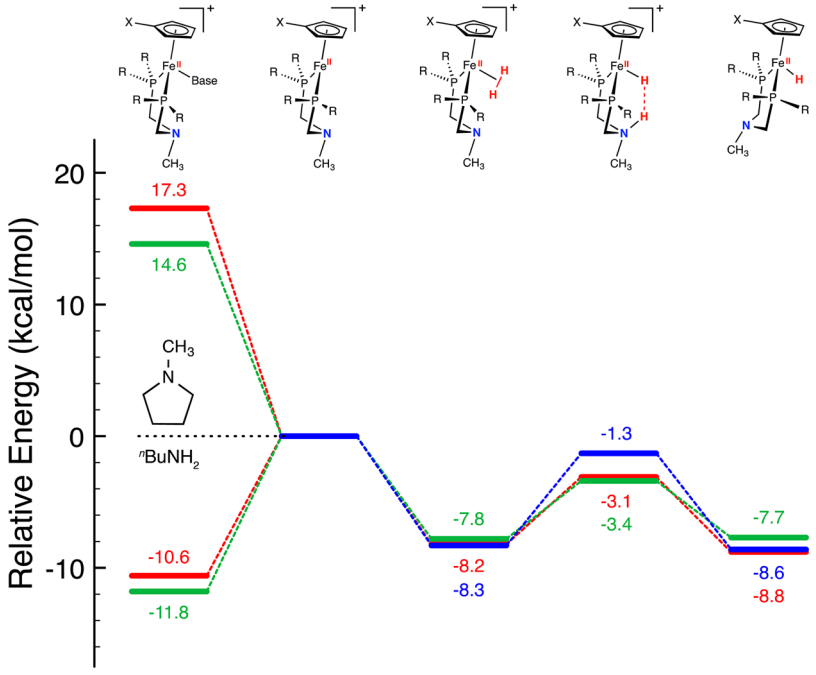

Figure 8. Free energy diagram for the reaction of the coordinatively unsaturated, 16-electron Fe^{II} species in the presence of dihydrogen and an exogenous base as a function of cyclopentadienyl and phosphorus substituents as obtained from DFT calculations. $(Cp^{C_5F_4N})Fe(P^{Et}N^{Me}P^{Et})$, red; $(Cp^{C_5F_4N})Fe(P^{Ph}N^{Me}P^{Ph})$, green; $(Cp^{H})Fe(P^{Ph}N^{Me}P^{Ph})$, blue.

dx.doi.org/10.1021/cs500290w | *ACS Catal.* 2014, 4, 1246−1260

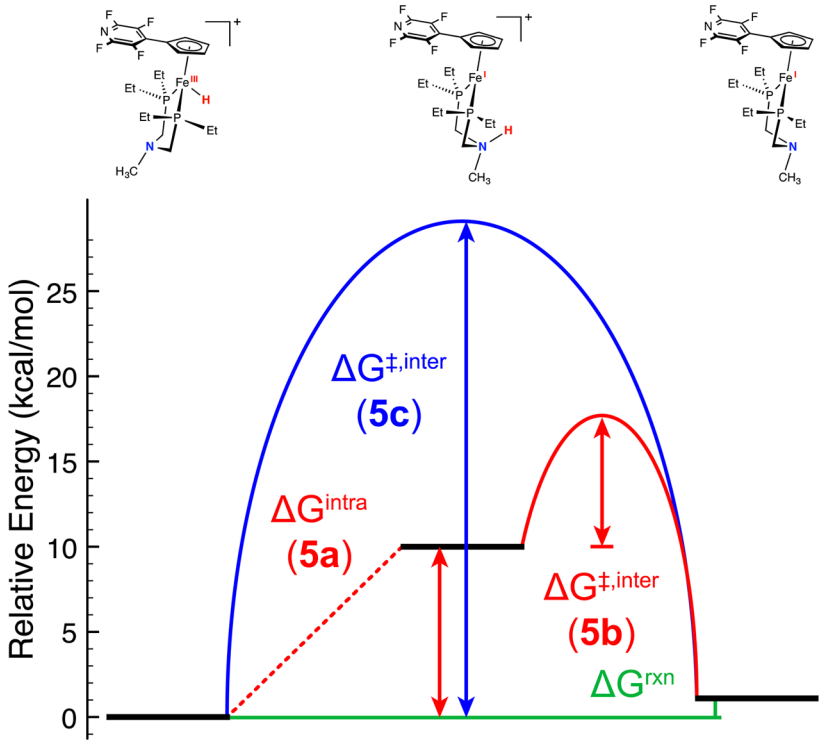

Figure 9. Free energy diagram for the intra- and intermolecular deprotonation of $[(Cp^{C_5F_4N})Fe(P^{Et}N^{Me}P^{Et})H]^+$ by *N*-methylpyrrolidine as obtained from DFT calculations. All reaction free energies and barriers are presented as solid lines. The blue line represents direct deprotonation of the Fe(III) hydride by the exogenous base (step 5c, Figure 6). The dashed and solid red lines represent deprotonation of the Fe(III) hydride by the pendant amine and subsequent deprotonation by the exogenous base (step 5a–b, Figure 6).

Table 5. Estimation of the Pseudo-First-Order Rate Constants for the Deprotonation of Fe^{III} Hydride Complexes With *N*-Methylpyrrolidine

compd	k_{est} (s^{-1})[a]
$(Cp^{C_5F_4N})Fe(P^{Ph}N^{Me}P^{Ph})(H)$	≫ 25
$(Cp^{C_5F_4N})Fe(P^{Et}N^{Me}P^{Et})(H)$	>25
$(Cp^{C_5F_4N})Fe(P^{Et}N^{Bn}P^{Et})(H)$	<2
$(Cp^{C_5F_4N})Fe(P^{Et}N^{tBu}P^{Et})(H)$	<2
$(Cp^{C_5F_4N})Fe(depp)(H)$	<0.1

[a]Conditions: 1 mM [Fe], 0.1 M $[^nBu_4N][B(C_6F_5)_4]$, fluorobenzene solution, 0.1 M *N*-methylpyrrolidine. Potentials are referenced to $Cp_2Fe^{+/0}$.

This behavior is in clear contrast to $[(Cp^{C_5F_4N})Fe(P^{Et}N^{R'}P^{Et})(H)]^+$ (R′ = ^{t}Bu, Bn), which show rate constants of <2 s^{-1} for the deprotonation of the Fe^{III} hydride species at 0.1 M *N*-methylpyrrolidine. These results are best explained by the ability of the proton relay to deprotonate the Fe^{III} hydride and transfer the proton to the exogenous base. In the case of R′ = ^{t}Bu, the pK_a is likely very similar to that of R′ = Me, indicating that steric interference is preventing deprotonation.[41] When R′ = Bn, the steric environment about the pendant amine is similar to that of R′ = Me, but the pK_a of the amine is likely 1–2 pK_a units lower.[41] In this case, the slow rate can be attributed to the inability of the amine to facilitate intramolecular deprotonation of the Fe^{III} hydride and relay the proton to the exogenous base.

In contrast to $[(Cp^{C_5F_4N})Fe(P^{Ph}N^{Me'}P^{Et})(H)]^+$, the unsubstituted cyclopentadienyl complex, $(Cp^{H})Fe(P^{Ph}N^{Me}P^{Ph})(H)$, does not show electrocatalytic oxidation of H_2 (see SI, Figure S7). This behavior is attributed to the decreased acidity of the Fe^{III} hydride, as compared with those incorporating electron-withdrawing substituents on the cyclopentadienyl ligand, thereby preventing its deprotonation. Computational data also indicate deprotonation of $(Cp^{H})Fe(P^{Ph}N^{Me}P^{Ph})(H)$ is significantly less favored than in the case of the $Cp^{C_5F_4N}$ derivatives (Figure 9).

Two iron analogs with bidentate diphosphine ligands without pendant amines (dppp and depp, where dppp = 1,3-bis(diphenylphosphino)propane, depp = 1,3-bis-(diethylphosphino)propane) were also prepared to probe the role of the proton relay in the catalytic pathway (Scheme 4).

Scheme 4. Control Complexes Prepared to Examine the Role of the Pendant Amine

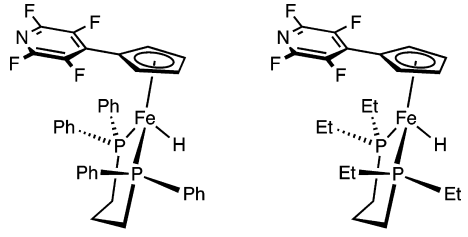

Characterization of each of these complexes and their precursors can be found in the Experimental Section. Although the unsaturated Fe^{II} derivatives react with H_2 in the presence of a strong base to form their respective hydrides, they are not electrocatalysts for the oxidation of H_2 (see SI, Figure S8). Electrochemical studies of the electrochemically generated Fe^{III}

dx.doi.org/10.1021/cs500290w | *ACS Catal.* 2014, 4, 1246–1260

hydride, $(Cp^{C_5F_4N})Fe(depp)(H)^+$, in the presence of 0.10 M *N*-methylpyrrolidine give an estimated pseudo-first-order rate constant for deprotonation by the exogenous base of <0.1 s^{-1}. Although direct deprotonation of electrochemically generated Fe^{III} hydrides is feasible without the pendant amine, the rate of deprotonation of the hydride by the exogenous base appears to be much slower than in the presence of the pendant amine. To increase the driving force for direct deprotonation of the Fe^{III} hydride, a stronger base, DBU (1,8-diaza-bicyclo[5.4.0]undec-7-ene, pK_a = 24 for H-DBU$^+$ in CH_3CN),[42] was used. In this case, deprotonation of $(Cp^{C_5F_4N})Fe(depp)(H)^+$ is facile, with an estimated rate constant of 20 s^{-1} assuming a pseudo-first-order process. These results show that although deprotonation of the Fe^{III} hydrides is feasible by a relatively strong exogenous base (Figure 6, step 5c), the kinetic route with a suitable pK_a-matched base is likely through deprotonation of the pendant amine after intramolecular proton transfer. Although use of a stronger exogenous base can facilitate the catalytic process, they can inhibit catalysis by binding to the metal.

Overall, the rate-determining steps in the electrocatalytic oxidation of H_2 by $[(Cp^{C_5F_4N})Fe(P^RN^{Me}P^R)]^+$ (R = Ph, Me) appear to be a combination of the deprotonation of the Fe^{III} hydride (Figure 6, step 5a–b) and competitive binding to the 16-electron Fe^{II} species by the exogenous base (Figure 6, step 7). At low base concentrations, the measured pseudo-first-order rate constant for the deprotonation of the Fe^{III} hydride is consistent with the overall observed TOF of the catalyst. However, when catalysis reaches the base concentration-independent region, this deprotonation process for $[(Cp^{C_5F_4N})Fe(P^RN^{Me}P^R)(H)]^+$ (*R* = Ph, Et) appears to be faster than the observed rate of catalysis. Strong base binding to the 16-electron Fe^{II} unsaturated species has been shown to occur with small bases such as ^{n}BuNH$_2$ and, although less favorable, with larger bases such as *N*-methylpyrrolidine. Under these conditions, the overall turnover frequency will be limited by the equilibrium between the 16-electron Fe^{II} species and its base-bound adduct.

CONCLUDING REMARKS

We have reported the synthesis of a new family of cyclopentadienyl iron complexes featuring $R_2PCH_2N(R')CH_2PR_2$ ligands and evaluated them for the electrocatalytic oxidation of H_2 at 1 atm of pressure. Two of the complexes, $(Cp^{C_5F_4N})Fe(P^{Ph}N^{Me}P^{Ph})(H)$ and $(Cp^{C_5F_4N})Fe(P^{Et}N^{Me}P^{Et})(H)$, were found to be active electrocatalysts, both of which are more active than the $P^R_2N^{R'}_2$ analogues. Mechanistic and computational investigations demonstrated the role of the PNP ligands in increasing the steric environment about the metal center and preventing the binding of bases with the sterically hindered, coordinating bases, such as *N*-methylpyrrolidine; however, slower intramolecular proton transfer rates were observed compared with the $P^R_2N^{R'}_2$ analogs previously reported. Analogs without the pendant base served as control complexes and demonstrated the importance of the pendant amine with respect to energy matching and facilitating proton transfer and heterolytic cleavage. Current efforts in our laboratory to increase the rate of intramolecular proton transfer through rational ligand modification to achieve better energy matching of the catalytic intermediates are currently underway.

EXPERIMENTAL SECTION

General Experimental Procedures. All manipulations with free phosphine ligands and metal reagents were carried out under argon using standard vacuum line, Schlenk, and inert atmosphere glovebox techniques. Solvents were purified by passage through neutral alumina using an Innovative Technology, Inc., PureSolv solvent purification system. THF-d_8 and bromobenzene-d_5 were purified by vacuum transfer from NaK and CaH_2, respectively, after stirring for a minimum of 24 h under an inert atmosphere. Photolysis reactions were conducted using a water-jacketed medium pressure mercury lamp (Ace Hanovia 450 W). All amines used for electrocatalysis were dried over KOH or CaH_2, degassed, distilled under vacuum, and stored in an argon-filled glovebox. Quartz glassware was used for all photolysis reactions. The following compounds were prepared according to literature procedures: $NaCp^{C_5F_4N}$,[36] $Ph_2PCH_2N(Me)CH_2PPh_2$,[43] $Et_2PCH_2N(Me)CH_2PEt_2$,[43] $Et_2PCH_2N(Bn)CH_2PEt_2$,[43] depp,[44] $(dppp)FeCl_2$,[45] $[CpFe(CO)_2Cl]$.[46]

Instrumentation. NMR spectra were recorded on a Varian Inova spectrometer (500 MHz for ^{1}H) at 22 °C unless otherwise noted. All ^{1}H chemical shifts have been internally calibrated using the monoprotio impurity of the deuterated solvent. The $^{31}P\{^1H\}$ NMR spectra were referenced to external phosphoric acid at 0 ppm. The ^{19}F NMR spectra were referenced to external fluorobenzene at −113.15 ppm. Peak widths at half heights are reported for paramagnetically broadened and shifted resonances.

All experimental procedures were conducted at ambient temperature, 23 °C, under argon using either standard Schlenk conditions or a Vacuum Atmospheres drybox. A standard three-electrode configuration was employed in conjunction with a CH Instruments potentiostat interfaced to a computer with CH Instruments 700 D software. All voltammetric scans were recorded using glassy-carbon working electrode disks of 1 mm diameter (Cypress Systems EE040). A glassy-carbon rod (Structure Probe, Inc.) and platinum wire (Alfa-Aesar) were used as auxiliary electrodes and quasi-reference electrodes, respectively. All glassware for electrochemical experiments was oven-dried overnight and allowed to cool to room temperature before use. $[Cp_2Co][PF_6]$ was used as an internal standard, and all potentials reported within this work are referenced to the cobaltocene/cobaltocenium couple at −1.33 V. Bases were measured and transferred to electrochemical solutions via gastight syringes.

Crystals selected for diffraction studies were immersed in Paratone-N oil, placed on a nylon loop, and transferred to a precooled cold stream of N_2. A Bruker KAPPA APEX II CCD diffractometer with 0.71073 Å Mo Kα radiation was used for diffraction studies. The space groups were determined on the basis of systematic absences and intensity statistics. The structures were solved by direct methods and refined by full-matrix least-squares on F^2. All non-hydrogen atoms were refined anisotropically unless otherwise stated. Hydrogen atoms were placed at idealized positions and refined using the riding model unless otherwise stated. Data collection and cell refinement were performed using Bruker APEX2 software. Data reductions and absorption corrections were performed using Bruker's SAINT and SADABS programs, respectively.[47,48] Structural solutions and refinements were completed using SHELXS-97 and SHELXL-97,[49] respectively, using the OLEX2 software package[50] as a front-end.

dx.doi.org/10.1021/cs500290w | ACS Catal. 2014, 4, 1246–1260

Ab Initio Calculations. Molecular structures were optimized without symmetry constrains within the density functional theory framework using the B3P86 exchange and correlation functional[51,52] in fluorobenzene described by the SMD solvation model.[53] The Stuttgart basis set with effective core potential was used for Ni atom, whereas the 6-311G* basis set was used for all of the other atoms with one additional p polarization funtion for the protic hydrogens. The optimized structures were confirmed by frequency calculations. Harmonic vibrational frequencies were calculated at the optimized geometries using the same level of theory to estimate the zero-point energy (ZPE) and the thermal contributions (298 K and 1 atm) to the gas-phase free energy. All calculations were carried out with the program Gaussian 09.[54]

Preparation of $Et_2PCH_2N(^tBu)CH_2PEt_2$. A 50 mL Schlenk flask was loaded with 0.34 g (11 mmol) of paraformaldehyde, approximately 10 mL of ethanol, and a stir bar. Cycling between vacuum and nitrogen degassed the vessel, and 1.3 mL (11 mmol) of diethylphosphine was added by syringe with rapid stirring. After 0.5 h, 0.70 mL (5.5 mmol) of *tert*-butylamine was added by syringe. The reaction was warmed to 65 °C and stirred for 2 days. The solvent was removed under vacuum, and 1.0 g (65% yield) of a colorless oil identified as $Et_2PCH_2N(^tBu)CH_2PEt_2$ was collected. $^1H\{^{31}P\}$ NMR (bromobenzene-d_5, 22 °C): δ 1.06 (t, 7.6 Hz, 12H, $P(CH_2CH_3)_2$), 1.12 (s, 9H, $NC(CH_3)_3$), 1.32 (dq, J = 13.9, 7.6 Hz, 4H, $P(CH_2CH_3)_2$), 1.43 (dq, J = 13.9, 7.6 Hz, 4H, $P(CH_2CH_3)_2$), 2.97 (s, 4H, NCH_2P). $^{13}C\{^1H\}$ NMR (bromobenzene-d_5, 22 °C): δ 9.9 (m, $P(CH_2CH_3)_2$), 18.4 (m, $P(CH_2CH_3)_2$), 27.4 (t, J_{CP} = 2 Hz, $NC(CH_3)_3$), 50.7 (t, J_{CP} = 4.2 Hz, NCH_2P), 54.6 (t, J_{CP} = 2.4 Hz, $NC(CH_3)_3$). $^{31}P\{^1H\}$ NMR (bromobenzene-d_5, 22 °C): δ −29.3.

Preparation of $Et_2PCH_2N(Ph)CH_2PEt_2$. The compound was prepared in a manner similar to $Et_2PCH_2N(^tBu)CH_2PEt_2$ with 0.34 g (11 mmol) of paraformaldehyde, 1.3 mL (11 mmol) of diethylphosphine, and 0.51 g (5.5 mmol) of aniline. Removal of solvent gave 1.38 g (85% yield) of a colorless oil identified as $Et_2PCH_2N(Ph)CH_2PEt_2$. ^1H NMR (benzene-d_6, 22 °C): δ 0.97 (dt, J = 13.6, 7.7 Hz, 12H, $P(CH_2CH_3)_2$), 1.16–1.37 (m, 8H, $P(CH_2CH_3)_2$), 3.26 (s, 4H, NCH_2P), 6.78 (t, J = 6.3 Hz, 1H, N*Ph*), 6.98 (d, J = 7.7 Hz, 2H, N*Ph*), 7.23 (t, J = 7.7 Hz, 2H, N*Ph*). $^{31}P\{^1H\}$ NMR (THF): δ −27.9 (s). $^{13}C\{^1H\}$ (benzene-d_6, 22 °C): δ 10.8 (d, J_{CP} = 14.9 Hz, $P(CH_2CH_3)_2$), 19.5 (d, J_{CP} = 13.0 Hz, $P(CH_2CH_3)_2$), 53.2–53.4 (m, NCH_2P), 116.5 (N*Ph*), 118.5 (N*Ph*), 129.8 (N*Ph*), 150.9 (N*Ph*).

Preparation of $(P^{Ph}N^{Me}P^{Ph})FeCl_2$. A 20 mL scintillation vial was charged with 0.14 g (1.1 mmol) of $FeCl_2$ and 3 mL of THF. A solution of 0.50 g (1.2 mmol) of $P^{Ph}N^{Me}P^{Ph}$ in 10 mL of THF was then added to the slurry with rapid stirring, causing a gradual color change to honey-yellow. After 24 h, the solvent was removed under vacuum, and the resulting solid was triturated with 15 mL of a 1:1 solution of pentane/diethyl ether. Filtration furnished 0.60 g (97% yield) of a pale yellow solid identified as $(P^{Ph}N^{Me}P^{Ph})FeCl_2$. Anal. Calcd for $C_{27}H_{27}P_2NFeCl_2$: C, 58.51; H, 4.91; N, 2.53. Found: C, 58.26; H, 5.07; N, 2.50. ^1H NMR (bromobenzene-d_5, 22 °C): δ −3.80 ($\nu_{1/2}$ = 200 Hz, 8H, PPh_2), −2.55 ($\nu_{1/2}$ = 1360 Hz, 4H, PPh_2 or NCH_2P), 5.04 ($\nu_{1/2}$ = 300 Hz, 4H, PPh_2 or NCH_2P), 14.90 ($\nu_{1/2}$ = 100 Hz, 8H, PPh_2), 109.97 ($\nu_{1/2}$ = 5370 Hz, 3H, NCH_3).

Preparation of $(P^{Et}N^{Me}P^{Et})FeCl_2$. The compound was prepared in a manner similar to $(P^{Ph}N^{Me}P^{Ph})FeCl_2$ with 0.23 g (0.98 mmol) of $P^{Et}N^{Me}P^{Et}$ and 0.12 g (0.93 mmol) of $FeCl_2$. Removal of solvent, trituration with a 1:1 solution of pentane/diethyl ether, and filtration gave 0.33 g (98% yield) of an off-white solid identified as $(P^{Et}N^{Me}P^{Et})FeCl_2$. Anal. Calcd for $C_{11}H_{27}P_2NFeCl_2$: C, 36.49; H, 7.52; N, 3.87. Found: C, 36.43; H, 7.25; N, 3.87. ^1H NMR (bromobenzene-d_5, 22 °C): δ 0.68 ($\nu_{1/2}$ = 815 Hz, 4H, NCH_2P), 4.62 ($\nu_{1/2}$ = 530 Hz, 4H, PCH_2N), 67.41 ($\nu_{1/2}$ = 1980 Hz, 4H, $P(CH_2CH_3)_2$), 93.28 ($\nu_{1/2}$ = 2475 Hz, 3H, NCH_3), 116.61 ($\nu_{1/2}$ = 1545 Hz, 4H, $P(CH_2CH_3)_2$).

Preparation of $(P^{Et}N^{Ph}P^{Et})FeCl_2$. The compound was prepared in a manner similar to $(P^{Ph}N^{Me}P^{Ph})FeCl_2$ with 0.24 g (0.81 mmol) of $P^{Et}N^{Ph}P^{Et}$ and 0.10 g (0.81 mmol) of $FeCl_2$. Removal of solvent, trituration with diethyl ether, and filtration gave 0.33 g (98% yield) of a yellow solid identified as $(P^{Et}N^{Ph}P^{Et})FeCl_2$. Anal. Calcd for $C_{16}H_{29}P_2NFeCl_2$: C, 45.31; H, 6.89; N, 3.30. Found: C, 45.57; H, 6.81; N, 3.13. ^1H NMR (bromobenzene-d_5, 22 °C): δ −0.730 ($\nu_{1/2}$ = 575 Hz, 14H, $P(CH_2CH_3)_2$ and NCH_2P), 6.82 ($\nu_{1/2}$ = 41 Hz, 2H, NCH_2P or N*Ph*), 7.35 ($\nu_{1/2}$ = 85 Hz, 1H, N*Ph*), 7.72 ($\nu_{1/2}$ = 55 Hz, 2H, NCH_2P or N*Ph*), 65.70 ($\nu_{1/2}$ = 1460 Hz, 4H, $P(CH_2CH_3)_2$), 101.11 ($\nu_{1/2}$ = 1950 Hz, 2H, N*Ph*), 126.97 ($\nu_{1/2}$ = 1600 Hz, 4H, $P(CH_2CH_3)_2$).

Preparation of $(P^{Et}N^{Bn}P^{Et})FeCl_2$. The compound was prepared in a manner similar to $(P^{Ph}N^{Me}P^{Ph})FeCl_2$ with 0.22 g (0.71 mmol) of $P^{Et}N^{Bn}P^{Et}$ and 0.089 g (0.71 mmol) of $FeCl_2$. Removal of solvent, trituration with diethyl ether, and filtration gave 0.29 g (95% yield) of an off-white solid identified as $(P^{Et}N^{Bn}P^{Et})FeCl_2$. Anal. Calcd for $C_{17}H_{31}P_2NFeCl_2$: C, 46.60; H, 7.13; N, 3.20. Found: C, 46.48; H, 6.89; N, 3.29. ^1H NMR (bromobenzene-d_5, 22 °C): δ 1.30 ($\nu_{1/2}$ = 540 Hz, 14H, $P(CH_2CH_3)_2$ and NCH_2P or NCH_2Ph), 5.57 ($\nu_{1/2}$ = 150 Hz, 2H, NCH_2P or NCH_2Ph), 7.18 ($\nu_{1/2}$ = 25 Hz, 1H, NCH_2Ph), 7.43 ($\nu_{1/2}$ = 31 Hz, 2H, NCH_2P or NCH_2Ph), 62.41 ($\nu_{1/2}$ = 1390 Hz, 4H, $P(CH_2CH_3)_2$), 93.64 ($\nu_{1/2}$ = 2730 Hz, 2H, NCH_2Ph), 115.31 ($\nu_{1/2}$ = 1045 Hz, 4H, $P(CH_2CH_3)_2$).

Preparation of $(P^{Et}N^{tBu}P^{Et})FeCl_2$. The compound was prepared in a manner similar to $(P^{Ph}N^{Me}P^{Ph})FeCl_2$ with 0.40 g (1.4 mmol) of $P^{Et}N^{tBu}P^{Et}$ and 0.18 g (1.4 mmol) of $FeCl_2$. Removal of solvent, trituration with diethyl ether, and filtration gave 0.47 g (98% yield) of an off-white solid identified as $(P^{Et}N^{tBu}P^{Et})FeCl_2$. Anal. Calcd for $C_{14}H_{33}P_2NFeCl_2$: C, 41.61; H, 8.23; N, 3.47. Found: C, 41.53; H, 8.24; N, 3.48. ^1H NMR (bromobezene-d_5, 22 °C): δ −0.97 ($\nu_{1/2}$ = 1020 Hz, 16H, $P(CH_2CH_3)_2$, and NCH_2P), 2.58 ($\nu_{1/2}$ = 340 Hz, 9H, $NC(CH_3)_3$), 62.33 ($\nu_{1/2}$ = 1935 Hz, 4H, $P(CH_2CH_3)_2$), 129.00 ($\nu_{1/2}$ = 1935 Hz, 4H, $P(CH_2CH_3)_2$).

Preparation of (depp)$FeCl_2$. The compound was prepared in a manner similar to $(P^{Ph}N^{Me}P^{Ph})FeCl_2$ with 0.29 g (1.3 mmol) of depp and 0.16 g (1.3 mmol) of $FeCl_2$. Removal of solvent, trituration with diethyl ether, and filtration gave 0.43 g (94% yield) of an off-white solid identified as (depp)$FeCl_2$. ^1H NMR (bromobenzene-d_5, 22 °C): δ 1.26 (465 Hz, 12H, $P(CH_2CH_3)_2$), 20.58 (445 Hz, 2H, $CH_2(CH_2P)_2$), 65.50 (950 Hz, 4H, $P(CH_2CH_3)_2$), 100.50 (915 Hz, 4H, $CH_2(CH_2P)_2$), 113.35 (1025 Hz, 4H, $P(CH_2CH_3)_2$).

Preparation of (Cp)Fe($P^{Ph}N^{Me}P^{Ph}$)(Cl). A 250 mL quartz flask was charged with 0.43 g (2.0 mmol) of $(Cp)Fe(CO)_2(Cl)$, 0.86 g (2.0 mmol) of $P^{Ph}N^{Me}P^{Ph}$, and 150 mL of toluene. The resulting solution what photolyzed for ∼15 h, yielding a color change from red to black. Reaction completion was confirmed by infrared and ^{31}P NMR spectroscopy. The solution was filtered through Celite to remove insoluble residues, and the

dx.doi.org/10.1021/cs500290w | ACS Catal. 2014, 4, 1246–1260

filtrate was evaporated under vacuum. Recrystallization of the product from 20 mL of toluene layered with 200 mL hexane afforded 0.84 g (70% yield) of black crystals identified as $(Cp)Fe(P^{Ph}N^{Me}P^{Ph})(Cl)$. ^1H NMR (toluene-d_8, 22 °C): δ 1.87 (s, 3H, NCH_3), 2.96 (dt, J_{HH} = 10 Hz, J_{PH} = 5 Hz, 2H, NCH_2P), 3.13 (J_{HH} = 10 Hz, J_{PH} = 5 Hz, 2H, NCH_2P), 4.04 (s, 5H, C_5H_5), 6.94−8.09 (m, 20H, PPh_2). $^{31}P\{^1H\}$ NMR (toluene-d_8, 22 °C): δ 57.0 (s).

Preparation of $(Cp^{C_5F_4N})Fe(P^{Ph}N^{Me}P^{Ph})(Cl)$. A 20 mL scintillation vial was charged with 0.30 g (0.54 mmol) of $(P^{Ph}N^{Me}P^{Ph})FeCl_2$, 5 mL of THF, and a stir bar and was stored at −35 °C for 20 min. A chilled (−35 °C for 20 min) solution of 0.12 g (0.51 mmol) of $NaCp^{C_5F_4N}$ in 10 mL of THF was then added dropwise with rapid stirring, and resulted in a color change from pale yellow to dark brown. The reaction mixture was stirred for 16 h, and the solvent was removed under vacuum. The residue was extracted with a 1:1 solution of diethyl ether/toluene and the resulting mixture was filtered through a pad of Celite. The solvent was removed under vacuum to afford 0.32 g (86% yield) of a dark brown solid identified as $(Cp^{C_5F_4N})Fe(P^{Ph}N^{Me}P^{Ph})(Cl)$. The product was recrystallized from diethyl ether to afford analytically pure material. $^1H\{^{31}P\}$ NMR (THF-d_8, 22 °C): δ 2.21 (s, 3H, NCH_3), 3.04−3.32 (m, 4H, NCH_2P), 3.90 (app. q, J = 1.8 Hz, 2H, $C_5H_4C_5F_4N$), 5.41 (app. q, J = 1.6 Hz, 2H, $C_5H_4C_5F_4N$), 7.14 (t, J = 7.3 Hz, 4H, PPh_2), 7.20−7.39 (m, 12H, PPh_2, 7.83 (d, J = 7.7 Hz, 4H, PPh_2). ^{31}P (THF-d_8, 22 °C): δ 50.0 (s). ^{19}F (THF-d_8, 22 °C): δ −139.2 (m), −96.0 (m).

Preparation of $(Cp^{C_5F_4N})Fe(P^{Et}N^{Me}P^{Et})(Cl)$. The compound was prepared in a manner similar to $(Cp^{C_5F_4N})Fe(P^{Ph}N^{Me}P^{Ph})$-(Cl) with 0.32 g (0.90 mmol) of $(P^{Et}N^{Me}P^{Et})FeCl_2$ and 0.21 g (0.90 mmol) of $NaCp^{C_5F_4N}$. Removal of solvent and recrystallization from diethyl ether gave 0.43 g (89% yield) of a dark green solid identified as $(Cp^{C_5F_4N})Fe(P^{Et}N^{Me}P^{Et})(Cl)$. Anal. Calcd for $C_{21}H_{31}F_4P_2N_2FeCl$: C, 46.65; H, 5.78; N, 5.18. Found: C, 46.85; H, 5.82; N, 5.27. $^1H\{^{31}P\}$ NMR (THF-d_8, 22 °C): δ 1.20 (t, J = 7.6 Hz, 6H, $P(CH_2CH_3)_2$), 1.21 (t, J = 7.6 Hz, 6H, $P(CH_2CH_3)_2$), 1.91−2.34 (m, 4H, $P(CH_2CH_3)_2$), 2.20 (d, J = 12.4 Hz, 2H, NCH_2P), 2.25 (s, 3H, NCH_3), 2.66 (d, J = 12.4 Hz, 2H, NCH_2P), 3.76 (app. t, J = 2.2 Hz, 2H, $C_5H_4C_5F_4N$), 5.44 (app. p, J = 2.0 Hz, 2H, $C_5H_4C_5F_4N$). ^{31}P (THF-d_8, 22 °C): δ 44.9 (s). ^{19}F (THF-d_8, 22 °C): δ −141.2 (m), −96.7 (m).

Preparation of $(Cp^{C_5F_4N})Fe(P^{Et}N^{Ph}P^{Et})(Cl)$. The compound was prepared in a manner similar to $(Cp^{C_5F_4N})Fe(P^{Ph}N^{Me}P^{Ph})$-(Cl) with 0.25 g (0.59 mmol) of $(P^{Et}N^{Ph}P^{Et})FeCl_2$ and 0.14 g (0.59 mmol) of $NaCp^{C_5F_4N}$. Removal of solvent and recrystallization from diethyl ether gave 0.29 g (89% yield) of a dark green solid identified as $(Cp^{C_5F_4N})Fe(P^{Et}N^{Ph}P^{Et})(Cl)$. $^1H\{^{31}P\}$ NMR (THF-d_8, 22 °C): δ 1.22 (t, J = 7.6 Hz, 6H, $P(CH_2CH_3)_2$), 1.25 (t, J = 7.6, 6H, $P(CH_2CH_3)_2$), 2.13 (q, J = 7.6 Hz, 4H, $P(CH_2CH_3)_2$), 2.19−2.48 (m, 4H, $P(CH_2CH_3)_2$), 2.94 (d, J = 13.2 Hz, 2H, NCH_2P), 3.59 (d, J = 13.2 Hz, 2H, NCH_2P), 3.86 (app. t, J = 2.1 Hz, 2H, $C_5H_4C_5F_4N$), 5.50 (app. p, J = 1.9 Hz, 2H, $C_5H_4C_5F_4N$), 6.82 (t, J = 7.3 Hz, 1H, *p-phenyl*), 6.96 (d, J = 7.9 Hz, 2H, *o-phenyl*), 7.19 (t, J = 7.9 Hz, 2H, *m-phenyl*). ^{31}P (THF-d_8, 22 °C): δ 45.2 (s). ^{19}F (THF-d_8, 22 °C): δ −140.97 (m), −96.57 (m).

Preparation of $(Cp^{C_5F_4N})Fe(P^{Et}N^{Bn}P^{Et})(Cl)$. The compound was prepared in a manner similar to $(Cp^{C_5F_4N})Fe(P^{Ph}N^{Me}P^{Ph})$-(Cl) with 0.25 g (0.57 mmol) of $(P^{Et}N^{Bn}P^{Et})FeCl_2$ and 0.14 g (0.57 mmol) of $NaCp^{C_5F_4N}$. Removal of solvent and recrystallization from diethyl ether gave 0.34 g (96% yield) of a dark green solid identified as $(Cp^{C_5F_4N})Fe(P^{Et}N^{Bn}P^{Et})(Cl)$. Anal. Calcd for $C_{27}H_{35}F_4P_2N_2FeCl$: C, 52.57; H, 5.72; N, 4.54. Found: C, 52.63; H, 5.68; N, 4.58. $^1H\{^{31}P\}$ NMR (THF-d_8, 22 °C): δ 0.99 (t, J = 7.6 Hz, 6H, $P(CH_2CH_3)_2$), 1.15 (t, J = 7.7 Hz, 6H, $P(CH_2CH_3)_2$), 1.84−2.06 (m, 4H, $P(CH_2CH_3)_2$), 2.04−2.28 (m, 4H, $P(CH_2CH_3)_2$), 2.25 (d, J = 12.6 Hz, 2H, NCH_2P), 2.81 (d, J = 12.6 Hz, 2H, NCH_2P), 3.45 (s, 2H, NCH_2Ph), 3.74 (app. t, J = 2.0 Hz, 2H, $C_5H_4C_5F_4N$), 5.42 (app. p, J = 1.8 Hz, 2H, $C_5H_4C_5F_4N$), 7.18−7.34 (m, 5H, NCH_2Ph). ^{31}P (THF-d_8, 22 °C): δ 44.9 (s). ^{19}F (THF-d_8, 22 °C): δ −141.2 (m), −96.8 (m).

Preparation of $(Cp^{C_5F_4N})Fe(P^{Et}N^{tBu}P^{Et})(Cl)$. The compound was prepared in a manner similar to $(Cp^{C_5F_4N})Fe$-$(P^{Ph}N^{Me}P^{Ph})(Cl)$ with 0.40 g (0.99 mmol) of $(P^{Et}N^{tBu}P^{Et})FeCl_2$ and 0.22 g (0.94 mmol) of $NaCp^{C_5F_4N}$. Removal of solvent and recrystallization from diethyl ether gave 0.52 g (95% yield) of a dark green solid identified as $(Cp^{C_5F_4N})Fe(P^{Et}N^{tBu}P^{Et})(Cl)$. Anal. Calcd for $C_{24}H_{37}F_4P_2N_2FeCl$: C, 49.46; H, 6.40; N, 4.81. Found: C, 49.71; H, 6.39; N, 4.77. $^1H\{^{31}P\}$ NMR (THF-d_8, 22 °C): δ 1.02 (s, 9H, $NC(CH_3)_3$), 1.21 (t, J = 7.7 Hz, 6H, $P(CH_2CH_3)_2$), 1.24 (t, J = 7.7 Hz, 6H, $P(CH_2CH_3)_2$), 2.04 (m, 4H, $P(CH_2CH_3)_2$), 2.10 (d, J = 12.4 Hz, 2H, NCH_2P), 2.22 (m, 4H, $P(CH_2CH_3)_2$), 3.07 (d, J = 12.4 Hz, 2H, NCH_2P), 3.81 (t, J = 2.0 Hz, 2H, $C_5H_4C_5F_4N$), 3.81 (app. t, J = 2.0 Hz, 2H, $C_5H_4C_5F_4N$), 5.44 (app. p, J = 1.9 Hz, 2H, $C_5H_4C_5F_4N$). ^{31}P (THF-d_8, 22 °C): δ 44.8 (s). ^{19}F (THF-d_8, 22 °C): δ −141.1 (m), −96.8 (m).

Preparation of $(Cp^{C_5F_4N})Fe(dppp)(Cl)$. The compound was prepared in a manner similar to $(Cp^{C_5F_4N})Fe(P^{Ph}N^{Me}P^{Ph})$-(Cl) with 0.45 g (0.83 mmol) of $(dppp)FeCl_2$ and 0.19 g (0.79 mmol) of $NaCp^{C_5F_4N}$. Removal of solvent and recrystallization from diethyl ether gave 0.53 g (93% yield) of a brown-black solid identified as $(Cp^{C_5F_4N})Fe(dppp)(Cl)$. $^1H\{^{31}P\}$ NMR (THF-d_8, 22 °C): δ 1.46 (qt, J = 14.3, 2.3 Hz, 1H, $CH_2(CH_2P)_2$), 2.02−2.11 (m, 1H, $CH_2(CH_2P)_2$), 2.16 (ddd, J = 14.0, 4.6, 2.3 Hz, 2H, $CH_2(CH_2P)_2$), 2.40 (td, J = 14.0, 3.7 Hz, 2H, $CH_2(CH_2P)_2$), 4.01 (app. t, J = 2.1 Hz, 2H, $C_5H_4C_5F_4N$), 5.30 (app. p, J = 1.7 Hz, 2H, $C_5H_4C_5F_4N$), 7.21−7.23 (m, 8H, PPh_2), 7.24−7.29 (m, 4H, PPh_2), 7.31−7.35 (m, 2H, PPh_2), 7.37−7.43 (m, 2H, PPh_2), 7.85−7.83 (m, 4H, PPh_2). ^{31}P (THF-d_8, 22 °C): δ 52.5 (s). ^{19}F (THF-d_8, 22 °C): δ −138.8 (m), −96.2 (m).

Preparation of $(Cp^{C_5F_4N})Fe(depp)(Cl)$. The compound was prepared in a manner similar to $(Cp^{C_5F_4N})Fe(P^{Ph}N^{Me}P^{Ph})$-(Cl) with 0.30 g (0.86 mmol) of $(depp)FeCl_2$ and 0.20 g (0.86 mmol) of $NaCp^{C_5F_4N}$. Removal of solvent and recrystallization from diethyl ether gave 0.41 g (90% yield) of a dark green solid identified as $(Cp^{C_5F_4N})Fe(depp)(Cl)$. $^1H\{^{31}P\}$ NMR (THF-d_8, 22 °C): δ 1.16 (t, J = 7.7 Hz, 6H, $P(CH_2CH_3)_2$), 1.21 (t, J = 7.6 Hz, 6H, $P(CH_2CH_3)_2$), 1.33 (td, J = 13.7, 1.8 Hz, 1H, $CH_2(CH_2P)_2$), 1.45 (ddd, J = 13.7, 4.4, 1.1 Hz, 2H, $CH_2(CH_2P)_2$), 1.59 (ddd, J = 13.4, 5.1, 1.7 Hz, 2H, $CH_2(CH_2P)_2$), 1.89 (dq, J = 15.3, 7.7 Hz, 2H, $P(CH_2CH_3)_2$), 1.93−2.00 (m, 1H, $CH_2(CH_2P)_2$), 2.45 (td, J = 15.2, 7.6 Hz, 2H, $P(CH_2CH_3)_2$), 2.24−2.38 (m, 4H, $P(CH_2CH_3)_2$), 3.76 (app. t, 2.1 Hz, 2H, $C_5H_4C_5F_4N$), 5.39 (app. p, 1.8 Hz, 2H, $C_5H_4C_5F_4N$). ^{31}P (THF-d_8, 22 °C): δ = 43.2 (s). ^{19}F (THF-d_8, 22 °C): δ = −141.08 (m), −96.85 (m).

Preparation of $(Cp^{C_5F_4N})Fe(P^{Ph}N^{Me}P^{Ph})(H)$. A 20 mL scintillation vial was charged with 0.20 g (0.27 mmol) of $(Cp^{C_5F_4N})Fe(P^{Ph}N^{Me}P^{Ph})(Cl)$, 0.10 g (2.7 mmol) of $NaBH_4$, and a stir bar. Ethanol (10 mL) was added with rapid stirring, resulting in the formation of H_2, and a gradual color change to

dx.doi.org/10.1021/cs500290w | ACS Catal. 2014, 4, 1246−1260

orange-red occurred. The reaction progress was monitored by ^{31}P NMR spectroscopy. Upon completion, the solvent was removed under vacuum, and the residue was extracted with diethyl ether. Filtration through a pad of Celite and removal of solvent under vacuum afforded 0.16 g (86% yield) of an orange solid identified as $(Cp^{C_5F_4N})Fe(P^{Ph}N^{Me}P^{Ph})(H)$. The product was further purified by recrystallization from pentane at −35 °C. Anal. Calcd for $C_{37}H_{32}F_4P_2N_2Fe$: C, 63.63; H, 4.62; N, 4.01. Found: C, 63.61; H, 4.81; N, 3.95. $^1H\{^{31}P\}$ NMR (THF-d_8, 22 °C): δ −15.38 (s, 1H, Fe*H*), 2.11 (s, 3H, NCH_3), 2.23 (d, J = 12.8 Hz, NCH_2P), 3.49 (d, J = 12.8 Hz, NCH_2P), 4.19 (app. t, J = 2.1 Hz, 2H, $C_5H_4C_5F_4N$), 5.06 (app. p, J = 2.0 Hz, 2H, $C_5H_4C_5F_4N$), 7.13−7.26 (m, 10H, P*Ph*), 7.32 (m, 2H, P*Ph*), 7.40−7.54 (m, 8H, P*Ph*). ^{31}P (THF-d_8, 22 °C): δ 73.7 (d, J_{PH} = 70 Hz). ^{19}F (THF-d_8, 22 °C): δ −142.63 (m), −97.01 (m).

Preparation of (Cp)Fe($P^{Ph}N^{Me}P^{Ph}$)(H). The compound was prepared in a manner similar to $(Cp^{C_5F_4N})Fe(P^{Ph}N^{Me}P^{Ph})$-(H) with 0.30 g (0.51 mmol) of $(Cp^{H})Fe(P^{Et}N^{Me}P^{Et})(Cl)$ and 0.19 g (5.1 mmol) of $NaBH_4$. Removal of solvent and recrystallization from diethyl ether gave 0.17 g (61% yield) of a yellow-orange solid identified as $(Cp^{H})Fe(P^{Ph}N^{Me}P^{Ph})(H)$. Anal. Calcd. for $C_{33}H_{33}N_2FeP_2$: C, 70.60; H, 5.92; N, 2.49. Found: C, 70.25; H, 6.29; N, 2.54. ^1H NMR (toluene-d_8, 22 °C): δ −16.24 (t, J_{PH} = 65.0 Hz, 1H, Fe*H*), 1.85 (s, 3H, NCH_3), 2.01 (d, J_{HH} = 15 Hz, 2H, NCH_2P), 3.32 (J_{HH} = 15 Hz, J_{PH} = 5 Hz, 2H, NCH_2P), 4.00 (s, 5H, C_5H_5), 6.96−7.76 (m, 20H, PPh_2). $^{31}P\{^1H\}$ (toluene-d_8, 22 °C): δ 76.7 (s).

Preparation of $(Cp^{C_5F_4N})Fe(P^{Et}N^{Me}P^{Et})(H)$. The compound was prepared in a manner similar to $(Cp^{C_5F_4N})Fe(P^{Ph}N^{Me}P^{Ph})$-(H) with 0.35 g (0.65 mmol) of $(Cp^{C_5F_4N})Fe(P^{Et}N^{Me}P^{Et})(Cl)$ and 0.24 g (6.5 mmol) of $NaBH_4$. Removal of solvent and recrystallization from diethyl ether gave 0.35 g (97% yield) of an intensely red solid identified as $(Cp^{C_5F_4N})Fe(P^{Et}N^{Me}P^{Et})(H)$. Anal. Calcd for $C_{21}H_{32}F_4P_2N_2Fe$: C, 49.82; H, 6.37; N, 5.53. Found: C, 50.05; H, 6.27; N, 5.62. $^1H\{^{31}P\}$ NMR (THF-d_8, 22 °C): δ −17.15 (s, 1H, Fe*H*), 0.90 (t, J = 7.6 Hz, 6H, P(CH_2CH_3)$_2$), 1.07 (t, J = 7.7 Hz, 6H, P(CH_2CH_3)$_2$), 1.39 (dq, J = 14.0, 7.8 Hz, 2H, P(CH_2CH_3)$_2$), 1.58 (dq, J = 14.9, 7.5 Hz, 2H, P(CH_2CH_3)$_2$), 1.64 (d, J = 12.9 Hz, 2H, NCH_2P), 1.70−1.83 (m, 2H, P(CH_2CH_3)$_2$), 2.17 (s, 3H, NCH_3), 2.74 (d, J = 12.3 Hz, 2H, NCH_2P), 4.51 (app. t, J = 2.0 Hz, 2H, $C_5H_4C_5F_4N$), 5.02 (app. p, J = 2.0 Hz, 2H, $C_5H_4C_5F_4N$). ^{31}P (THF-d_8, 22 °C): δ 65.5 (d, J_{PH} = 72 Hz). ^{19}F (THF-d_8, 22 °C): δ −144.74 (m), −96.81 (m).

Preparation of $(Cp^{C_5F_4N})Fe(P^{Et}N^{Ph}P^{Et})(H)$. The compound was prepared in a manner similar to $(Cp^{C_5F_4N})Fe(P^{Ph}N^{Me}P^{Ph})$-(H) with 0.20 g (0.33 mmol) of $(Cp^{C_5F_4N})Fe(P^{Et}N^{Ph}P^{Et})(Cl)$ and 0.13 g (3.3 mmol) of $NaBH_4$. Removal of solvent and recrystallization from diethyl ether gave 0.18 g (94% yield) of an intensely red solid identified as $(Cp^{C_5F_4N})Fe(P^{Et}N^{Ph}P^{Et})(H)$. $^1H\{^{31}P\}$ NMR (THF-d_8, 22 °C): δ −16.69 (s, 1H, Fe*H*), 0.96 (t, J = 7.6 Hz, 6H, P(CH_2CH_3)$_2$), 1.11 (t, J = 7.7 Hz, 6H, P(CH_2CH_3)$_2$), 1.49 (dq, J = 14.2, 7.8 Hz, 2H, P(CH_2CH_3)$_2$), 1.69 (dq, J = 14.9, 7.4 Hz, 2H, P(CH_2CH_3)$_2$), 1.76−1.92 (m, 4H, P(CH_2CH_3)$_2$), 2.49 (d, J = 13.1 Hz, NCH_2P), 3.70 (d, J = 13.5 Hz, NCH_2P), 4.59 (app. t, J = 2.1 Hz, 2H, $C_5H_4C_5F_4N$), 5.07 (app. p, J = 2.1 Hz, 2H, $C_5H_4C_5F_4N$), 6.75 (t, J = 7.3 Hz, 1H, *p-Ph*), 6.85 (d, J = 7.9 Hz, 2H, *o-Ph*), 7.11−7.17 (m, 2H, *m-Ph*). ^{31}P (THF-d_8, 22 °C): δ 66.7 (d, J_{PH} = 70 Hz). ^{19}F (THF-d_8, 22 °C): δ −144.5 (m), −96.6 (m).

Preparation of $(Cp^{C_5F_4N})Fe(P^{Et}N^{Bn}P^{Et})(H)$. The compound was prepared in a manner similar to $(Cp^{C_5F_4N})Fe(P^{Ph}N^{Me}P^{Ph})$-(H) with 0.25 g (0.40 mmol) of $(Cp^{C_5F_4N})Fe(P^{Et}N^{Bn}P^{Et})(Cl)$ and 0.15 g (4.0 mmol) of $NaBH_4$. Removal of solvent and recrystallization from diethyl ether gave 0.22 g (94% yield) of an intensely red solid identified as $(Cp^{C_5F_4N})Fe(P^{Et}N^{Bn}P^{Et})(H)$. Anal. Calcd for $C_{27}H_{36}F_4P_2N_2Fe$: C, 55.68; H, 6.23; N, 4.81. Found: C, 55.83; H, 6.33; N, 4.70. $^1H\{^{31}P\}$ NMR (THF-d_8, 22 °C): δ −17.11 (s, 1H, Fe*H*), 0.88 (t, J = 7.4 Hz, 6H, P(CH_2CH_3)$_2$), 0.91 (t, J = 7.8 Hz, 6H, P(CH_2CH_3)$_2$), 1.35 (dq, J = 15.3, 7.8 Hz, 2H, P(CH_2CH_3)$_2$), 1.53 (dq, J = 14.7, 7.4 Hz, 2H, P(CH_2CH_3)$_2$), 1.68−1.77 (m, 6H, P(CH_2CH_3)$_2$ and NCH_2P), 2.87 (d, J = 12.5 Hz, 2H, NCH_2P), 3.38 (s, 2H, NCH_2Ph), 4.51 (app. t, J = 2.2 Hz, 2H, $C_5H_4C_5F_4N$), 5.00 (app. p, J = 2.2 Hz, 2H, $C_5H_4C_5F_4N$), 7.15−7.31 (m, 5H, NCH_2*Ph*). ^{31}P (THF-d_8, 22 °C): δ 65.6 (d, J_{PH} = 71 Hz). ^{19}F (THF-d_8, 22 °C): δ −144.75 (m), −96.8 (m).

Preparation of $(Cp^{C_5F_4N})Fe(P^{Et}N^{tBu}P^{Et})(H)$. The compound was prepared in a manner similar to $(Cp^{C_5F_4N})Fe(P^{Ph}N^{Me}P^{Ph})$-(H) with 0.25 g (0.43 mmol) of $(Cp^{C_5F_4N})Fe(P^{Et}N^{tBu}P^{Et})(Cl)$ and 0.16 g (4.3 mmol) of $NaBH_4$. Removal of solvent and recrystallization from diethyl ether gave 0.23 g (96% yield) of an intensely red solid identified as $(Cp^{C_5F_4N})Fe(P^{Et}N^{tBu}P^{Et})(H)$. Anal. Calcd for $C_{24}H_{38}F_4P_2N_2Fe$: C, 52.57; H, 6.98; N, 5.11. Found: C, 52.57; H, 7.17; N, 5.05. $^1H\{^{31}P\}$ NMR (THF-d_8, 22 °C): δ −16.83 (s, 1H, Fe*H*), 0.90 (t, J = 7.6 Hz, 6H, P(CH_2CH_3)$_2$), 0.96 (s, 9H, NC(CH_3)$_3$), 1.12 (t, J = 7.7 Hz, 6H, P(CH_2CH_3)$_2$), 1.41 (dq, J = 15.5, 7.8 Hz, 2H, P(CH_2CH_3)$_2$), 1.57 (dq, J = 14.8, 7.4 Hz, 2H, P(CH_2CH_3)$_2$), 1.67 (d, J = 12.2 Hz, 2H, NCH_2P), 1.75 (dd, J = 15.5, 7.8 Hz, 4H, P(CH_2CH_3)$_2$), 3.14 (d, J = 12.2 Hz, 2H, NCH_2P), 4.53 (app. t, J = 2.1 Hz, 2H, $C_5H_4C_5F_4N$), 5.01 (app. p, J = 2.1 Hz, 2H, $C_5H_4C_5F_4N$). ^{31}P (THF-d_8, 22 °C): δ 66.1 (d, J_{PH} = 72 Hz). ^{19}F (THF-d_8, 22 °C): δ −144.8 (m), −96.9 (m).

Preparation of $(Cp^{C_5F_4N})Fe(dppp)(H)$. The compound was prepared in a manner similar to $(Cp^{C_5F_4N})Fe(P^{Ph}N^{Me}P^{Ph})(H)$ with 0.50 g (0.69 mmol) of $(Cp^{C_5F_4N})Fe(dppp)(Cl)$ and 0.26 g (6.9 mmol) of $NaBH_4$. Removal of solvent and recrystallization from diethyl ether gave 0.33 g (69% yield) of a dark orange solid identified as $(Cp^{C_5F_4N})Fe(dppp)(H)$. $^1H\{^{31}P\}$ NMR (THF-d_8, 22 °C): δ −15.11 (t, J = 72 Hz, 1H, FeH), 1.12 (q, J = 14.0 Hz, 1H, $CH_2(CH_2P)_2$), 1.78 (td, J = 13.6, 2.8 Hz, 2H, $CH_2(CH_2P)_2$), 1.96 (bd, J = 14.0 Hz, 1H, $CH_2(CH_2P)_2$), 2.49 (dd, J = 14.1, 4.9 Hz, 2H, $CH_2(CH_2P)_2$), 4.35 (bs, 2H, $C_5H_4C_5F_4N$), 4.77 (bs, 2H, $C_5H_4C_5F_4N$), 7.05−7.24 (m, 6H, PPh_2), 7.28 (t, J = 7.4 Hz, 4H, *m-Ph*), 7.35 (t, J = 7.3 Hz, 2H *p-Ph*), 7.37−7.43 (m, 4H, PPh_2), 7.57 (d, J = 7.4 Hz, 4H, *o-Ph*). ^{31}P (THF-d_8, 22 °C): δ 73.3 (dd, J = 72, 29 Hz). ^{19}F (THF-d_8, 22 °C): δ −142.2 (m), −97.0 (m).

Preparation of $(Cp^{C_5F_4N})Fe(depp)(H)$. The compound was prepared in a manner similar to $(Cp^{C_5F_4N})Fe(P^{Ph}N^{Me}P^{Ph})(H)$ with 0.30 g (0.57 mmol) of $(Cp^{C_5F_4N})Fe(depp)(Cl)$ and 0.22 g (5.7 mmol) of $NaBH_4$. Removal of solvent and recrystallization from diethyl ether gave 0.27 g (95% yield) of an intensely red solid identified as $(Cp^{C_5F_4N})Fe(depp)(H)$. Anal. Calcd for $C_{21}H_{31}F_4P_2NFe$: C, 51.34; H, 6.36; N, 2.85. Found: C, 51.58; H, 6.20; N, 2.93. $^1H\{^{31}P\}$ NMR (THF-d_8, 22 °C): δ −16.76 (s, FeH), 0.91 (td, J = 7.6, 1.0 Hz, 6H, P(CH_2CH_3)$_2$), 1.01 (td, J = 13.3, 3.1 Hz, 2H, $CH_2(CH_2P)_2$), 1.06 (td, J = 7.7, 1.1 Hz, 6H, P(CH_2CH_3)$_2$), 1.33−1.44 (m, 3H, P(CH_2CH_3)$_2$ and $CH_2(CH_2P)_2$), 1.55−1.66 (m, 4H, P(CH_2CH_3)$_2$ and $CH_2(CH_2P)_2$), 1.73 (q, J = 7.7 Hz, 4H, P(CH_2CH_3)$_2$), 1.91 (dtt, J = 12.3, 6.0, 3.2 Hz, 1H, $CH_2(CH_2P)_2$), 4.52 (app. q, 1.9 Hz, 2H, $C_5H_4C_5F_4N$), 4.92 (app. dq, J = 4.1, 2.2 Hz). ^{31}P

dx.doi.org/10.1021/cs500290w | ACS Catal. 2014, 4, 1246−1260

(THF-d_8, 22 °C): δ 63.5 (d, J_{PH} = 73 Hz). ^{19}F (THF-d_8, 22 °C): δ −144.7 (m), −96.9 (m).

Preparation of [($Cp^{C_5F_4N}$)Fe($P^{Et}N^{Me}P^{Et}$)(H_2)][BAr^F_4]. A 100 mL round-bottom flask was charged with 0.20 g (0.37 mmol) of ($Cp^{C_5F_4N}$)Fe($P^{Et}N^{Me}P^{Et}$)(Cl) and 0.34 g (0.39 mmol) of $NaBAr^F_4$. Fluorobenzene (∼15 mL) was added with rapid stirring under an atmosphere of H_2, and a color change from deep green to orange-yellow was observed over the course of 10−15 min. After 1 h, the mixture was filtered through a pad of Celite. Addition of ∼45 mL of pentane precipitated the product, which was collected by filtration and dried under vacuum to afford 0.44 g (86% yield) of an orange-yellow crystalline solid identified as [($Cp^{C_5F_4N}$)Fe($P^{Et}N^{Me}P^{Et}$)(H_2)]-[BAr^F_4]. Anal. Calcd for $C_{53}H_{45}BF_{28}P_2N_2Fe$: C, 46.45; H, 3.31; N, 2.04. Found: C, 46.99; H, 3.32; N, 2.07. ^{1}H{^{31}P} NMR (bromobenzene-d_5, 22 °C): δ −13.74 (bs, Fe(H_2)), 0.58 (t, J = 7.6 Hz, 6H, P(CH_2CH_3)$_2$), 0.75 (t, 7.6 Hz, 6H, P(CH_2CH_3)$_2$), 1.03 (d, 13.8 Hz, 2H, NCH_2P), 1.27 (td, J = 15.8, 8.02 Hz, 2H, P(CH_2CH_3)$_2$), 1.40−1.62 (m, 6H, P(CH_2CH_3)$_2$), 1.82 (s, 3H, NCH_3), 2.39 (d, J = 13.8 Hz, 2H, NCH_2P), 4.22 (app. t, J = 1.9 Hz, 2H, $C_5H_4C_5F_4N$), 5.03 (app. s, 2H, $C_5H_4C_5F_4N$), 7.62 (s, 4H, BAr^F_4), 8.19 (app. s, 8H, BAr^F_4). ^{31}P (bromobenzene-d_5, 22 °C): δ 51.1 (s).

Preparation of [($Cp^{C_5F_4N}$)Fe($P^{Et}N^{Me}P^{Et}$)($NH_2{}^nBu$)][BAr^F_4]. A 20 mL scintillation vial was charged with 0.15 g (0.28 mmol) of ($Cp^{C_5F_4N}$)Fe($P^{Et}N^{Me}P^{Et}$)(Cl) and 0.26 g (0.29 mmol) of $NaBAr^F_4$. Fluorobenzene (∼15 mL) was added with rapid stirring. After 30 min, ^{n}BuNH_2 (27 μL, 0.28 mmol) was added by microsyringe, causing an immediate color change to brown. After 3 h, the reaction mixture was filtered through a pad of Celite, and pentane (∼60 mL) was added, causing the product to precipitate from solution. Vacuum filtration and washing with pentane furnished 0.36 g (91% yield) of a crystalline brown solid identified as [($Cp^{C_5F_4N}$)Fe($P^{Et}N^{Me}P^{Et}$)($NH_2{}^nBu$)]-[BAr^F_4]. Anal. Calcd for $C_{57}H_{54}F_{28}N_3P_2BFe$: C, 47.49; H, 3.78; N, 2.91. Found: C, 47.42; H, 3.69; N, 2.86. ^{1}H{^{31}P} NMR (bromobenzene-d_5, 22 °C): δ = 0.61 (t, J = 6.9 Hz, 3H, $NH_2CH_2(CH_2)_2CH_3$), 0.69−0.97 (m, 16H, P(CH_2CH_3)$_2$ and $NH_2CH_2(CH_2)_2CH_3$), 1.36 (qd, J = 15.2, 7.7 Hz, 4H, P(CH_2CH_3)$_2$), 1.50−1.74 (m, 6H, P(CH_2CH_3)$_2$ and $NH_2CH_2(CH_2)_2CH_3$), 1.83 (s, 3H, NCH_3), 1.85−1.96 (m, 2H, $NH_2CH_2(CH_2)_2CH_3$), 2.09 (d, J = 14 Hz, 2H, NCH_2P), 2.23 (d, J = 14 Hz, 2H, NCH_2P), 3.71 (app. t, J = 2.0 Hz, 2H, $C_5H_4C_5F_4N$), 4.90 (app. p, J = 2.0 Hz, 2H, $C_5H_4C_5F_4N$), 7.61 (s, 4H, BAr^F_4), 8.19 (s, 8H, BAr^F_4). ^{31}P (bromobenzene-d_5, 22 °C): δ = 44.3 (s).

Electrochemical H_2 oxidation catalyzed by (Cp^X)Fe($P^RN^{R'}P^R$)(H). A 1.0 mL fluorobenzene solution containing 1.0 mM (Cp^X)Fe($P^RN^{R'}P^R$)(H) under 1.0 atm H_2 was prepared. A cyclic voltammogram was recorded to obtain the peak current observed in the absence of an exogenous base. Aliquots of base were then added by microsyringe, and a cyclic voltammogram was recorded at 25 °C after each addition. Alternatively, electrocatalysis can be conducted starting with (Cp^X)Fe($P^RN^{R'}P^R$)(Cl) and the addition of $NaBAr^F_4$ to generate the 16-electron [(Cp^X)Fe($P^RN^{R'}P^R$)]$^+$ complexes.

Bulk Electrolysis. Bulk electrolysis was performed using a high-power BASi potentiostat with a four-necked flask. One neck was sealed with a rubber septum through which a copper wire was fed that pierced through a cylinder of reticulated vitreous carbon and functioned as the working electrode. The second and third necks were equipped with a reference electrode and a counter electrode suspended from copper wire that was fed through rubber septa. A AgCl-coated silver wire suspended in a 0.1 M fluorobenzene solution of [^{n}Bu$_4$N][B(C_6F_5)$_4$] in a glass tube with a Vycor frit served as the reference electrode. The counter electrode consisted of a Ni−Cr coiled wire and a 0.1 M fluorobenzene solution of [^{n}Bu$_4$N][B(C_6F_5)$_4$] in a glass tube with a glass frit. The fourth neck was fitted with a septum through which a copper wire attached to a second working electrode (1 mm PEEK-encased glassy carbon, Cpress Systems EE040) was fed. The second working electrode was used to record cyclic voltammograms. A needle was placed through this septum to introduce H_2 into the cell. The flask contained 20 mL of a 0.1 M [^{n}Bu$_4$N][B(C_6F_5)$_4$] solution in fluorobenzene as well as the catalyst, ($Cp^{C_5F_4N}$)Fe($P^{Et}N^{Me}P^{Et}$)-(H) (1.0 mM), and a small amount of Cp_2CoPF_6 (∼0.9 mM) as an internal reference. Before and after adding *N*-methylpyrrolidine (150 μL, 72 mM), two cyclic voltammograms were recorded to ensure that the solution was under catalytic condition and to determine the applied potential for bulk electrolysis. Controlled-potential electrolysis was performed at ∼0.1 V positive of the peak potential for ($Cp^{C_5F_4N}$)Fe($P^{Et}N^{Me}P^{Et}$)(H). After the application of 24.01 C of charge (corresponding to 6.3 calculated turnovers), a 200 μL aliquot of the solution was removed and mixed with 400 μL of a 20 mM solution of Verkade's base (2,8,9-triisopropyl-2,5,8,9-tetraaza-1-phosphabicyclo[3.3.3]undecane, 30 mg dissolved in 5 mL tetrahydrofuran). Verkade's base (pK_a of the conjugate acid = 33.6 in CH_3CN)[55] sequestered all protons from the protonated *N*-methylpyrrolidine (pK_a of the conjugate acid = 18.02 in CH_3CN) produced from bulk electrolysis, forming protonated Verkade's base. The amount of Verkade's base (δ 118.0) and protonated Verkade's base (δ −11.9) can be quantified by ^{31}P{^{1}H} NMR spectroscopy, on the basis of the known concentration of the base. The amount of protons generated (14.0 mM in a 20 mL solution, 0.242 mmol, corresponding to 6.14 turnovers) from the oxidation of H_2 can be determined. A second sample was taken after passing 27.55 C of charge (corresponding to 7.2 calculated turnovers), giving the amount of protons as 18.3 mM in a 20 mL solution (0.266 mmol, corresponding to 6.7 turnovers). Faradic efficiencies of 97 and 93% were calculated for H_2 oxidation.

■ ASSOCIATED CONTENT

Ⓢ Supporting Information

Additional experimental details, including the preparation of $NaCp^{C_5F_4N}$, metrical parameters for [($Cp^{C_5F_4N}$)Fe($P^{Et}N^{Me}P^{Et}$)-($NH_2{}^nBu$)]$^+$, and electrochemical and electrocatalytic data. This material is available free of charge via the Internet at http://pubs.acs.org.

■ AUTHOR INFORMATION

Corresponding Author

*E-mail: monte.helm@pnnl.gov.

Notes

The authors declare no competing financial interest.

■ ACKNOWLEDGMENTS

This research was supported as part of the Center for Molecular Electrocatalysis, an Energy Frontier Research Center funded by the U.S. Department of Energy, Office of Science, Office of Basic Energy Sciences. Pacific Northwest National

Laboratory is operated by Battelle for the U.S. Department of Energy.

REFERENCES

(1) Lewis, N. S.; Nocera, D. G. *Proc. Natl. Acad. Sci. U.S.A.* **2006**, *103*, 15729−15735.
(2) Jacobson, M. Z.; Delucchi, M. A. *Energy Policy* **2011**, *39*, 1154−1169.
(3) Du, P.; Eisenberg, R. *Energy Environ. Sci.* **2012**, *5*, 6012−6021.
(4) Thoi, V. S.; Sun, Y.; Long, J. R.; Chang, C. J. *Chem. Soc. Rev.* **2013**, *42*, 2388−2400.
(5) Wang, M.; Chen, L.; Sun, L. *Energy Environ. Sci.* **2012**, *5*, 6763−6778.
(6) Yang, C.-J. *Energy Policy* **2009**, *37*, 1805−1808.
(7) Alonso, E.; Sherman, A. M.; Wallington, T. J.; Everson, M. P.; Field, F. R.; Roth, R.; Kirchain, R. E. *Environ. Sci. Technol.* **2012**, *46*, 3406−3414.
(8) *Catalysis without Precious Metals*, 1st ed.; Bullock, R. M., Ed.; Wiley-VCH: Weinheim, 2010.
(9) Bullock, R. M. *Science* **2013**, *342*, 1054−1055.
(10) Frey, M. *ChemBioChem* **2002**, *3*, 153−160.
(11) Camara, J. M.; Rauchfuss, T. B. *Nat. Chem.* **2012**, *4*, 26−30.
(12) Wang, N.; Wang, M.; Wang, Y.; Zheng, D.; Han, H.; Ahlquist, M. S. G.; Sun, L. *J. Am. Chem. Soc.* **2013**, *135*, 13688−13691.
(13) Fontecilla-Camps, J. C.; Volbeda, A.; Cavazza, C.; Nicolet, Y. *Chem. Rev.* **2007**, *107*, 4273−4303.
(14) Cracknell, J. A.; Vincent, K. A.; Armstrong, F. A. *Chem. Rev.* **2008**, *108*, 2439−2461.
(15) Vincent, K. A.; Parkin, A.; Armstrong, F. A. *Chem. Rev.* **2007**, *107*, 4366−4413.
(16) Shaw, W. J.; Helm, M. L.; DuBois, D. L. *Biochim. Biophys. Acta, Bioenerg.* **2013**, *1827*, 1123−1139.
(17) Bullock, R. M.; Appel, A. M.; Helm, M. L. *Chem. Commun.* **2014**, *50*, 3125−3143.
(18) DuBois, D. L.; Bullock, R. M. *Eur. J. Inorg. Chem.* **2011**, *2011*, 1017−1027.
(19) Liu, T.; DuBois, D. L.; Bullock, R. M. *Nat. Chem.* **2013**, *5*, 228−233.
(20) Wiedner, E. S.; Roberts, J. A. S.; Dougherty, W. G.; Kassel, W. S.; DuBois, D. L.; Bullock, R. M. *Inorg. Chem.* **2013**, *52*, 9975−9988.
(21) Wiedner, E. S.; Appel, A. M.; DuBois, D. L.; Bullock, R. M. *Inorg. Chem.* **2013**, *52*, 14391−14403.
(22) Rakowski DuBois, M.; DuBois, D. L. *Chem. Soc. Rev.* **2009**, *38*, 62−72.
(23) Henry, R. M.; Shoemaker, R. K.; DuBois, D. L.; Rakowski DuBois, M. *J. Am. Chem. Soc.* **2006**, *128*, 3002−3010.
(24) Liu, T.; Chen, S.; O'Hagan, M. J.; Rakowski DuBois, M.; Bullock, R. M.; DuBois, D. L. *J. Am. Chem. Soc.* **2012**, *134*, 6257−6272.
(25) Curtis, C. J.; Miedaner, A.; Ciancanelli, R.; Ellis, W. W.; Noll, B. C.; Rakowski DuBois, M.; DuBois, D. L. *Inorg. Chem.* **2003**, *42*, 216−227.
(26) Wilson, A. D.; Newell, R. H.; McNevin, M. J.; Muckerman, J. T.; Rakowski DuBois, M.; DuBois, D. L. *J. Am. Chem. Soc.* **2006**, *128*, 358−366.
(27) Raugei, S.; Chen, S.; Ho, M.-H.; Ginovska-Pangovska, B.; Rousseau, R. J.; Dupuis, M.; DuBois, D. L.; Bullock, R. M. *Chem.—Eur. J.* **2012**, *18*, 6493−6506.
(28) Franz, J. A.; O'Hagan, M. J.; Ho, M.-H.; Liu, T.; Helm, M. L.; Lense, S.; DuBois, D. L.; Shaw, W. J.; Appel, A. M.; Raugei, S.; Bullock, R. M. *Organometallics* **2013**, *32*, 7034−7042.
(29) Savéant, J. M. *Acc. Chem. Res.* **1980**, *13*, 323−329.
(30) Savéant, J. M.; Vianello, E. *Electrochim. Acta* **1965**, *10*, 905−920.
(31) Savéant, J. M.; Vianello, E. *Electrochim. Acta* **1967**, *12*, 629−646.
(32) Nicholson, R. S.; Shain, I. *Anal. Chem.* **1964**, *36*, 706−723.
(33) Roberts, J. A. S.; Bullock, R. M. *Inorg. Chem.* **2013**, *52*, 3823−3835.
(34) Appel, A. M.; Helm, M. L. *ACS Catal.* **2014**, *4*, 630−633.
(35) Hulley, E. B.; Welch, K. D.; Appel, A. M.; DuBois, D. L.; Bullock, R. M. *J. Am. Chem. Soc.* **2013**, *135*, 11736−11739.
(36) Liu, T.; Wang, X.; Hoffmann, C.; DuBois, D. L.; Bullock, R. M. *Angew. Chem., Int. Ed.* **2014**, DOI: 10.1002/anie.201402090.
(37) Ciancanelli, R.; Noll, B. C.; DuBois, D. L.; Rakowski DuBois, M. *J. Am. Chem. Soc.* **2002**, *124*, 2984−2992.
(38) Raebiger, J. W.; DuBois, D. L. *Organometallics* **2005**, *24*, 110−118.
(39) Chen, S.; Rousseau, R. J.; Raugei, S.; Dupuis, M.; DuBois, D. L.; Bullock, R. M. *Organometallics* **2011**, *30*, 6108−6118.
(40) Ryan, O. B.; Tilset, M.; Parker, V. D. *J. Am. Chem. Soc.* **1990**, *112*, 2618−2626.
(41) Izutsu, K. *Acid-Base Dissociation Constants in Dipolar Aprotic Solvents*; Blackwell Scientific Publications: Oxford, Boston, 1990.
(42) Kaljurand, I.; Kütt, A.; Sooväli, L.; Rodima, T.; Mäemets, V.; Leito, I.; Koppel, I. A. *J. Org. Chem.* **2005**, *70*, 1019−1028.
(43) Weiss, C. J.; Groves, A. N.; Mock, M. T.; Dougherty, W. G.; Kassel, W. S.; Helm, M. L.; DuBois, D. L.; Bullock, R. M. *Dalton Trans.* **2012**, *41*, 4517−4529.
(44) Curtis, C. J.; Miedaner, A.; Ellis, W. W.; DuBois, D. L. *J. Am. Chem. Soc.* **2002**, *124*, 1918−1925.
(45) Argouarch, G.; Hamon, P.; Toupet, L.; Hamon, J.-R.; Lapinte, C. *Organometallics* **2002**, *21*, 1341−1348.
(46) Piper, T. S.; Cotton, F. A.; Wilkinson, G. *J. Inorg. Nucl. Chem.* **1955**, *1*, 165−174.
(47) *SAINT Program for Data Reduction*; Bruker AXS Inc.: Madison, WI, USA, 2007.
(48) *SADABS Program for Absorption Correction of Area Detector Frames*; Bruker ASX Inc.: Madison, WI, USA, 2007.
(49) Sheldrick, G. *Acta Crystallogr. A* **2008**, *64*, 112−122.
(50) Dolomanov, O. V.; Bourhis, L. J.; Gildea, R. J.; Howard, J. A. K.; Puschmann, H. *J. Appl. Crystallogr.* **2009**, *42*, 339−341.
(51) Perdew, J. P. *Phys. Rev. B* **1986**, *33*, 8822−8824.
(52) Becke, A. D. *J. Chem. Phys.* **1993**, *98*, 5648.
(53) Marenich, A. V.; Cramer, C. J.; Truhlar, D. G. *J. Chem. Theory Comput.* **2009**, *5*, 2447−2464.
(54) Frisch, M. J.; Trucks, G. W.; Schlegel, H. B.; Scuseria, G. E.; Robb, M. A.; Cheeseman, J. R.; Scalmani, G.; Barone, V.; Mennucci, B.; Petersson, G. A.; Nakatsuji, H.; Caricato, M.; Li, X.; Hratchian, H. P.; Izmaylov, A. F.; Bloino, J.; Zheng, G.; Sonnenberg, J. L.; Hada, M.; Ehara, M.; Toyota, K.; Fukuda, R.; Hasegawa, J.; Ishida, M.; Nakajima, T.; Honda, Y.; Kitao, O.; Nakai, H.; Vreven, T.; Montgomery, J. A.; Peralta, J. E.; Ogliaro, F.; Bearpark, M.; Heyd, J. J.; Brothers, E.; Kudin, K. N.; Staroverov, V. N.; Kobayashi, R.; Normand, J.; Raghavachari, K.; Rendell, A.; Burant, J. C.; Iyengar, S. S.; Tomasi, J.; Cossi, M.; Rega, N.; Millam, J. M.; Klene, M.; Knox, J. E.; Cross, J. B.; Bakken, V.; Adamo, C.; Jaramillo, J.; Gomperts, R.; Stratmann, R. E.; Yazyev, O.; Austin, A. J.; Cammi, R.; Pomelli, C.; Ochterski, J. W.; Martin, R. L.; Morokuma, K.; Zakrzewski, V. G.; Voth, G. A.; Salvador, P.; Dannenberg, J. J.; Dapprich, S.; Daniels, A. D.; Farkas, Ö.; Foresman, J. B.; Ortiz, J. V.; Cioslowski, J.; Fox, D. J. *Gaussian 09, Revision B01*; Gaussian, Inc.: Wallingford, CT, 2009.
(55) Kisanga, P. B.; Verkade, J. G.; Schwesinger, R. *J. Org. Chem.* **2000**, *65*, 5431−5432.